Rapid assessment of Watson-Crick to Hoogsteen exchange in unlabeled DNA duplexes using high-power SELOPE imino ^{1}H CEST

Bei Liu[1], Atul Rangadurai[1], Honglue Shi[2], and Hashim M. Al-Hashimi*[1,2]

1. Department of Biochemistry, Duke University School of Medicine, Durham, NC, USA

2. Department of Chemistry, Duke University, Durham, NC, USA

**Correspondence to: hashim.al.hashimi@duke.edu*

Abstract. In duplex DNA, Watson-Crick A-T and G-C base pairs (bps) exist in dynamic equilibrium with an alternative Hoogsteen conformation, which is low in abundance and short-lived. Measuring how the Hoogsteen dynamics varies across different DNA sequences, structural contexts and physiological conditions is key for identifying potential Hoogsteen hot spots and for understanding the potential roles of Hoogsteen base pairs in DNA recognition and repair. However, such studies are hampered by the need to prepare ^{13}C or ^{15}N isotopically enriched DNA samples for NMR relaxation dispersion (RD) experiments. Here, using SELective Optimized Proton Experiments (SELOPE) ^{1}H CEST experiments employing high-power radiofrequency fields (B_1 > 250 Hz) targeting imino protons, we demonstrate accurate and robust characterization of Waston-Crick to Hoogsteen exchange, without the need for isotopic enrichment of the DNA. For 13 residues in three DNA duplexes under different temperature and pH conditions, the exchange parameters deduced from high-power imino ^{1}H CEST were in very good agreement with counterparts measured using off-resonance $^{13}C/^{15}N$ spin relaxation in the rotating frame ($R_{1\rho}$). It is shown that ^{1}H-^{1}H NOE effects which typically introduce artifacts in ^{1}H based measurements of chemical exchange can be effectively suppressed by selective excitation, provided that the relaxation delay is short (≤100 ms). The ^{1}H CEST experiment can be performed with ~10X higher throughput and ~100X lower cost relative to $^{13}C/^{15}N$ $R_{1\rho}$, and enabled Hoogsteen

chemical exchange measurements undetectable by $R_{1\rho}$. The results reveal an increased propensity to form Hoogsteen bps near terminal ends and a diminished propensity within A-tract motifs. The ^{1}H CEST experiment provides a basis for rapidly screening Hoogsteen breathing in duplex DNA, enabling identification of unusual motifs for more in-depth characterization.

1 Introduction

Soon after the discovery of the DNA double helix, it was shown that A-T and G-C could also pair in an alternative conformation known as the “Hoogsteen” base pair (bp) (Felsenfeld et al., 1957; Hoogsteen, 1959) (Fig. 1a). Starting from a canonical Watson-Crick G-C or A-T bp, the corresponding Hoogsteen bp can be obtained by flipping the purine base 180º and bringing the two bases into proximity to create a new set of hydrogen-bonds, which in the case of G-C bps require protonation of cytosine-N3 (Fig. 1a).

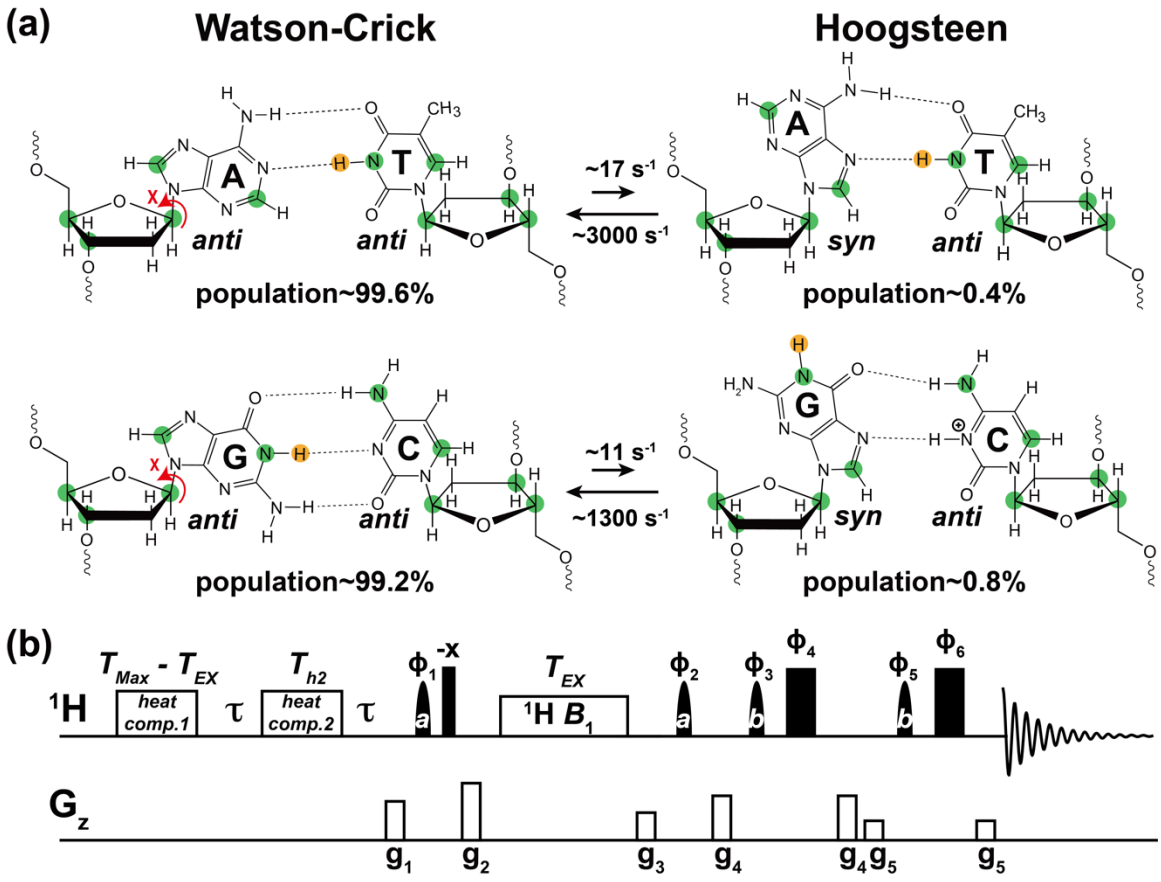

Figure 1. Using ^{1}H CEST to measure Watson-Crick to Hoogsteen exchange in unlabeled nucleic acid duplexes. (a) Watson-Crick G-C and A-T bps in B-DNA exist in dynamic equilibrium with G-C^{+} and A-T Hoogsteen bps, respectively. Filled green circles denote nuclei (^{13}C and ^{15}N) that have previously been used to probe the Watson-Crick to Hoogsteen exchange via RD measurements, while the yellow circle denotes the imino ^{1}H probes used in this study. Rate constants and populations were obtained as described previously (Alvey et al., 2014). (b) The 1D SELOPE ^{1}H CEST pulse sequence for characterizing chemical exchange in unlabeled nucleic acids. Narrow and wide filled rectangles denote 90° and 180°

hard pulses. Semi-oval shapes denote selective pulses. Pulse **a** is a 90° Eburp2.1000 shape pulse (typically 3-4 ms) for selective excitation (excitation bandwidth ~2-3 ppm) of imino protons, while pulse **b** is a 180° Squa100.1000 shape pulse with length 2 ms in an excitation sculpting scheme (Hwang and Shaka, 1995) for water suppression. Open rectangles denote the gradients and heat compensation elements. Delay τ = ½ d_1 = 0.7 s. To ensure uniform heating for experiments with variable lengths of T_{EX}, the relaxation period during which a ^{1}H B_1 field is applied, two heat compensation modules were used according to a prior study (Schlagnitweit et al., 2018). The first heat compensation is applied far off-resonance with duration = T_{Max} - T_{EX} = 2 ms, where T_{Max} is the maximum relaxation delay time. The second heat compensation (1 kHz) applied far off-resonance has a duration T_{h2} = 150 ms. The phase cycles used are ϕ_1 = {8x, 8(-x)}, ϕ_2 = {4x, 4(-x)}, ϕ_3 = {x, y}, ϕ_4 = {-x, -y}, ϕ_5 = {2x, 2y}, and ϕ_6 = {2(-x), 2(-y)}. Gradients (g1 - g5) with SMSQ10.100 profiles are applied for 1 ms with the following amplitudes (G cm^{-1}): 14.445, 26.215, 14.445, 16.585, 5.885. The ^{1}H carrier is placed far offset (100,000 Hz) during the two heat compensation periods, then moved to the center of the imino resonances prior to the first pulse **a.** Next, the carrier is placed to a specified offset prior to the relaxation delay (T_{EX}), then placed back to the center of the imino resonances following T_{EX}. Finally, it is placed on-resonance with water for water suppression prior to pulse **b**. Briefly, imino ^{1}H

magnetization is selectively excited, aligned longitudinally and then relaxes under a ^{1}H B_1 field during T_{EX}. ^{1}H transverse magnetization is then created and directly detected following water suppression. This pulse sequence is adapted from Schlagnitweit *et al* (Schlagnitweit et al., 2018).

Following their discovery, Hoogsteen bps were observed in crystal structures of duplex DNA in complex with proteins (Kitayner et al., 2010; Aishima et al., 2002) and drugs (Wang et al., 1984; Ughetto et al., 1985) and shown to play roles in DNA recognition (Golovenko et al., 2018), damage induction (Xu et al., 2020), and repair (Lu et al., 2010), and in damage bypass during replication (Nair et al., 2006; Ling et al., 2003). NMR relaxation dispersion (RD) studies employing off-resonance ^{13}C and ^{15}N spin relaxation in the rotating frame ($R_{1\rho}$) later showed that the G-C and A-T Watson-Crick bps exist in a dynamic equilibrium with their Hoogsteen counterparts (Nikolova et al., 2011). The Hoogsteen bps were shown to be lowly populated (population < 1 %) and short-lived (lifetime ~ 1 ms) forming robustly as an excited conformational state (ES) in duplex DNA across a variety of sequence contexts (Alvey et al., 2014) (Fig. 1a).

There is growing interest in mapping the Watson-Crick to Hoogsteen exchange landscape cross different DNA contexts, including for bps in different sequence

motifs (Alvey et al., 2014), near sites of damage and mismatches (Shi et al., 2021; Singh et al., 1993), and when DNA is bound to proteins (Nikolova et al., 2013b; Zhou et al., 2019) and drugs (Xu et al., 2018; Wang et al., 1984). Studies suggest an increased propensity to form Hoogsteen bps in such environments (Shi et al., 2021) and this may in turn play roles in DNA recognition and damage repair (Afek et al., 2020). Furthermore, there is interest in understanding how the Hoogsteen exchange varies with temperature (Nikolova et al., 2011), pH (Nikolova et al., 2013a), salt concentration and buffer composition (Rangadurai et al., 2020b; Tateishi-Karimata et al., 2014), as well as in the presence of epigenetic modifications (Wang et al., 2017; Rangadurai et al., 2019a), all of which could shape these dynamics and consequently DNA biochemical transactions.

There are hundreds and thousands of motifs and conditions for which characterization of Hoogsteen dynamics is of biological interest. However, current approaches for measuring Hoogsteen dynamics are ill-suited for dynamics measurements at such a scale. The Watson-Crick to Hoogsteen chemical exchange process has been characterized with the use of ^{13}C (Nikolova et al., 2011; Shi et al., 2018; Ben Imeddourene et al., 2020; Alvey et al., 2014) and ^{15}N (Nikolova et al., 2012a; Rangadurai et al., 2019a; Alvey et al., 2014) off-resonance $R_{1\rho}$, and more recently chemical exchange saturation transfer (CEST) experiments

(Rangadurai et al., 2020b; Rangadurai et al., 2020a). However, these approaches require isotopically enriched DNA samples, making broad explorations of Hoogsteen exchange across even tens of motifs impractical. Furthermore, many motifs of interest involve damaged or modified nucleotides, which are difficult to isotopically enrich with ^{13}C and ^{15}N nuclei. It is therefore desirable to have more facile means to initially assess Watson-Crick to Hoogsteen exchange, and to follow up with in-depth characterization for those motifs exhibiting interesting and unusual behavior. For such an initial screening application, we turned our attention to the imino ^{1}H as a probe of the Watson-Crick to Hoogsteen exchange in unlabeled DNA samples.

The utility of protons as probes in CEST (Chen et al., 2016; Dubini et al., 2020; Wang et al., 2021; Liu et al., 2020), Carr-Purcell-Meiboom-Gill (CPMG) (Juen et al., 2016; Leblanc et al., 2018), and off-resonance $R_{1\rho}$ experiments (Wang and Ikuta, 1989; Lane et al., 1993; Steiner et al., 2016; Schlagnitweit et al., 2018; Baronti et al., 2020; Furukawa et al., 2021) to study conformational exchange in nucleic acids is now well-established. Many of these ^{1}H based approaches use experiments originally developed to study conformational exchange in proteins (Ishima et al., 1998; Eichmuller and Skrynnikov, 2005; Lundstrom and Akke, 2005; Lundstrom et al., 2009; Otten et al., 2010; Bouvignies and Kay, 2012; Hansen et

al., 2012; Weininger et al., 2012; Weininger et al., 2013; Smith et al., 2015; Sekhar et al., 2016; Yuwen et al., 2017a; Yuwen et al., 2017b). The ^{1}H experiments permit the use of higher effective fields allowing characterization of conformational exchange faster than is possible using ^{13}C or ^{15}N experiments (Steiner et al., 2016; Palmer, 2014). Furthermore, the relationship between ^{1}H chemical shifts and structure is reasonably well understood and has been exploited in the conformational characterization of nucleic acids (Sripakdeevong et al., 2014; Frank et al., 2013; Wang et al., 2021; Swails et al., 2015; Czernek et al., 2000; Lam and Chi, 2010).

Recently, ^{1}H $R_{1\rho}$ and CEST SELective Optimized Proton Experiments (SELOPE) were developed and applied to characterize conformational exchange in unlabeled RNA (Schlagnitweit et al., 2018). The SELOPE experiment has already found several applications in studies of unlabeled nucleic acids, including in the characterization of fast ($k_{ex} = k_1 + k_{-1} > 1{,}000$ s^{-1}) RNA secondary structural rearrangements (Baronti et al., 2020) and DNA base opening (Furukawa et al., 2021), as well as slower ($k_{ex} < 100$ s^{-1}) DNA hybridization kinetics (Dubini et al., 2020). Many ^{1}H relaxation dispersion (RD) studies have targeted exchangeable imino protons (Baronti et al., 2020; Furukawa et al., 2021), taking advantage of the

well-known dependence of the imino ^{1}H chemical shifts on secondary structure (Wang et al., 2021; Lam and Chi, 2010).

Although ^{1}H RD experiments can obviate the need for isotopic labeling and offer other advantages such as high sensitivity, they have not been as widely used compared to ^{13}C/^{15}N RD experiments. One reason for this has to do with potential artifacts arising due to from ^{1}H-^{1}H cross relaxation (Ishima et al., 1998; Eichmuller and Skrynnikov, 2005; Lundstrom and Akke, 2005; Bouvignies and Kay, 2012). Interestingly, in nucleic acids, such NOE effects appear to be effectively suppressed in the ^{1}H SELOPE experiment through selective excitation of spins (Schlagnitweit et al., 2018). The exchange parameters obtained using ^{1}H SELOPE experiments were shown to be in very good agreement with counterparts obtained using ^{13}C and ^{15}N off-resonance $R_{1\rho}$ (Baronti et al., 2020). In addition, similar exchange parameters were obtained when using variable tilt angles in $R_{1\rho}$ experiments, including tilt angle of 35.3° in which ROE and NOE cross-relaxation terms cancel (Eichmuller and Skrynnikov, 2005; Weininger et al., 2013; Steiner et al., 2016). No NOE dips or artifacts were observed in the majority of the ^{1}H CEST or off-resonance $R_{1\rho}$ profiles (Steiner et al., 2016; Dubini et al., 2020; Furukawa et al., 2021). These results are consistent with a prior off-resonance ^{1}H $R_{1\rho}$ studies showing that even without deuteration, it is feasible to effectively suppress cross-

relaxation between amide and aliphatic protons through selective inversion of amide protons and use of short spin lock relaxation delays (Lundstrom and Akke, 2005; Schlagnitweit et al., 2018). Nevertheless, NOE effects have been reported for select sites in ^{1}H SELOPE studies of nucleic acids (Schlagnitweit et al., 2018), and in ^{1}H CEST studies of proteins (Bouvignies and Kay, 2012; Sekhar et al., 2016; Yuwen et al., 2017a; Yuwen et al., 2017b). This underscores the need to carefully analyze NOE effects, especially for unlabeled samples, in which spin-state-selective magnetization transfer schemes (Yuwen et al., 2017a; Yuwen et al., 2017b) employing heteronuclei to suppress NOE effects are not feasible.

There are certain conditions in which the Hoogsteen bp becomes the dominant conformation in duplex DNA. These include chemically modified bases (Nikolova et al., 2011), when DNA is in complex with binding partners (Xu et al., 2018), and for specific sequence contexts under certain experimental conditions (Stelling et al., 2017). Based on NMR studies of such duplexes containing Hoogsteen bps, there should be a sizeable difference ($\Delta\omega$ ~-1 – -2 ppm) between the imino proton chemical shifts of guanine (G-H1) and thymine (T-H3) in the Hoogsteen versus Watson-Crick conformation. These differences should render G-H1 and T-H3 suitable probes of Hoogsteen exchange in unlabeled DNA duplexes provided that NOE effects can be effectively suppressed. Imino protons are also attractive

probes given that they are often well-resolved even in 1D ^{1}H spectra of large RNAs. Since no other ESs have been detected to date in several NMR studies of unmodified canonical DNA duplexes (Nikolova et al., 2011; Alvey et al., 2014; Shi et al., 2018; Ben Imeddourene et al., 2020), a single imino ^{1}H probe could be sufficient to reliably map and characterize the Watson-Crick to Hoogsteen exchange.

Here, we show that high power ^{1}H CEST SELOPE experiments targeting the imino protons G-H1 and T-H3 provide facile means for initially assessing Watson-Crick to Hoogsteen exchange of G-C and A-T bps in DNA without the need for isotopic enrichment. NOE effects are shown to have a negligible contribution as short ($\leq$100 ms) relaxation delays can be used to characterize the relatively fast (k_{ex} ~ 500 to 8,000 s^{-1}) Watson-Crick to Hoogsten exchange process (Alvey et al., 2014). The approach also takes advantage of high-power radio-frequency (RF) fields recently shown (Rangadurai et al., 2020a) to extend the timescale sensitivity of CEST to include faster exchange processes that traditionally are more effectively characterized with the use of $R_{1\rho}$. The high-power ^{1}H CEST experiment also enabled measurement of fast Hoogsteen exchange kinetics (k_{ex} > 20,000 s^{-1}) inaccessible to conventional ^{13}C or ^{15}N off-resonance $R_{1\rho}$ RD. The ^{1}H CEST experiment opens the door to more comprehensively and systematically exploring

how the Watson-Crick to Hoogsteen exchange process varies with sequence and structural contexts, and physiological conditions of interest.

2 Results

2.1 Assessment of NOE effects

We used the SELOPE (Schlagnitweit et al., 2018) experiment (Fig. 1b) to measure ^{1}H CEST profiles for G-H1 and T-H3 in unlabeled DNA duplexes (Fig. 2) at 25 °C-26 °C. We used ^{1}H CEST rather than $R_{1\rho}$ given the greater ease of collecting profiles for many spins simultaneously, and given that with the use of high-power RF fields, CEST can effectively characterize exchange processes over a wide range of timescales (Rangadurai et al., 2020a). Use of high power RF fields was recently shown to be important to effectively characterize the comparatively fast (k_{ex} ~ 3,000 s^{-1}) Watson-Crick to Hoogsteen exchange process using ^{13}C and ^{15}N CEST experiments (Rangadurai et al., 2020a). Here, we also employed high power RF fields (> 250 Hz) to optimally characterize Watson-Crick to Hoogsteen exchange using ^{1}H CEST.

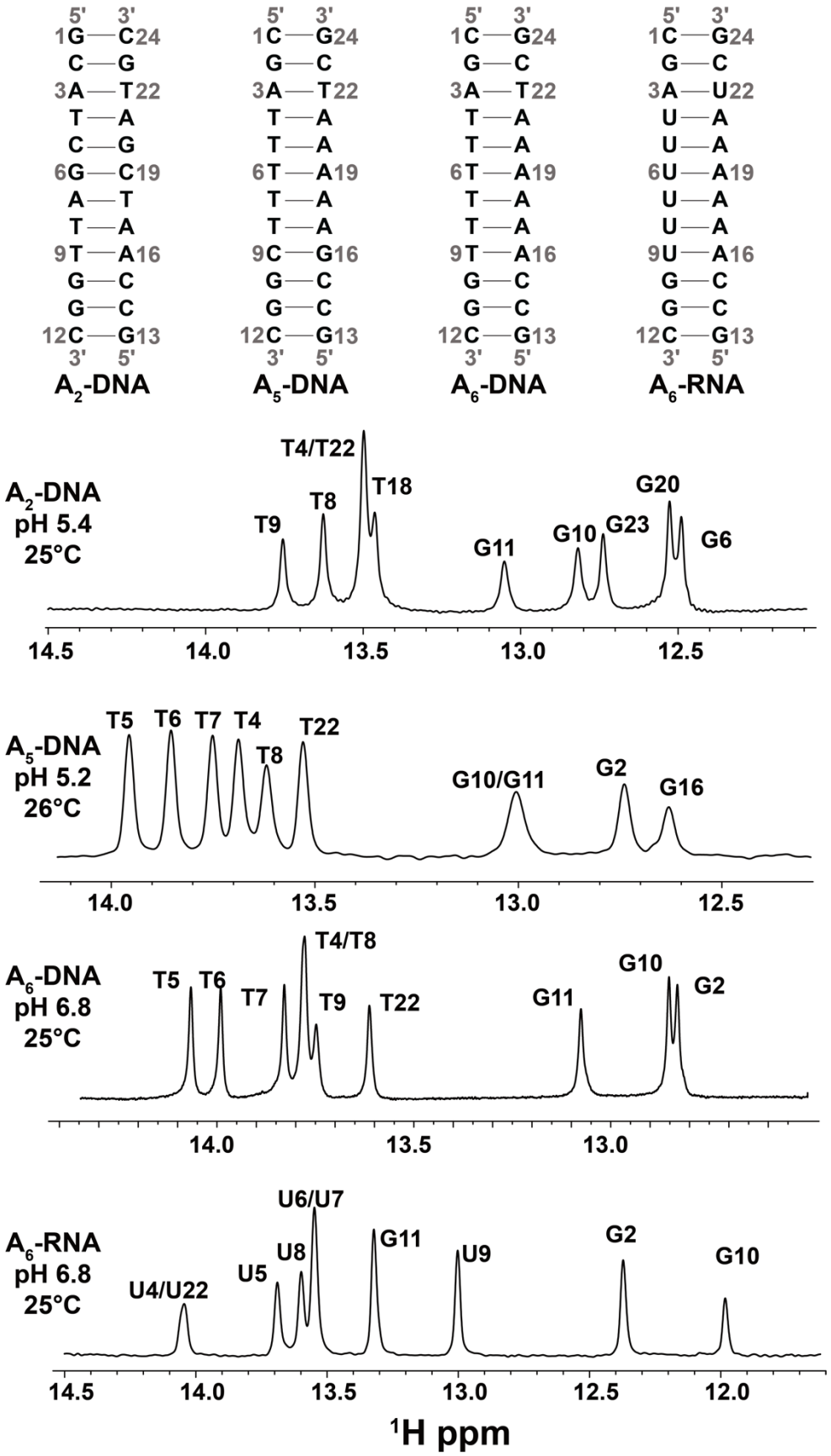
5' 3'
1G—C24
C—G
3A—T22
T—A
C—G
6G—C19
A—T
T—A
9T—A16
G—C
G—C
12C—G13
3' 5'
A2-DNA
5' 3'
1C—G24
G—C
3A—T22
T—A
T—A
6T—A19
T—A
T—A
9C—G16
G—C
G—C
12C—G13
3' 5'
A5-DNA
5' 3'
1C—G24
G—C
3A—T22
T—A
T—A
6T—A19
T—A
T—A
9T—A16
G—C
G—C
12C—G13
3' 5'
A6-DNA
5' 3'
1C—G24
G—C
3A—U22
U—A
U—A
6U—A19
U—A
U—A
9U—A16
G—C
G—C
12C—G13
3' 5'
A6-RNA
A2-DNA
pH 5.4
25°C
T4/T22
T8
T18
T9
G11
G10
G23
G20
G6
14.5
14.0
13.5
13.0
12.5
A5-DNA
pH 5.2
26°C
T5
T6
T7
T4
T8
T22
G10/G11
G2
G16
14.0
13.5
13.0
12.5
A6-DNA
pH 6.8
25°C
T5
T6
T7
T4/T8
T9
T22
G11
G10
G2
14.0
13.5
13.0
A6-RNA
pH 6.8
25°C
U4/U22
U5
U8
U6/U7
G11
U9
G2
G10
14.5
14.0
13.5
13.0
12.5
12.0
1H ppm

231

Figure 2. DNA and RNA duplexes used in this study. Also shown are 1D ^{1}H spectra of the imino region. The buffer conditions were 25 mM sodium chloride, 15 mM sodium phosphate, 0.1 mM EDTA and 10 % D_2O. The pH and temperature are indicated on each spectrum.

An important consideration when performing ^{1}H CEST experiments are contributions due to ^{1}H-^{1}H cross-relaxation, which may give rise to extraneous NOE dips in the ^{1}H CEST profiles (Ishima et al., 1998; Lundstrom and Akke, 2005; Eichmuller and Skrynnikov, 2005; Bouvignies and Kay, 2012; Sekhar et al., 2016; Yuwen et al., 2017a; Yuwen et al., 2017b). These contributions have been suppressed in proteins through deuteration (Eichmuller and Skrynnikov, 2005; Lundstrom and Akke, 2005; Lundstrom et al., 2009; Otten et al., 2010; Hansen et al., 2012; Weininger et al., 2012), and in ^{15}N isotopically labelled proteins (Yuwen et al., 2017a; Yuwen et al., 2017b) and nucleic acids (Wang et al., 2021; Liu et al., 2020) using spin-state-selective magnetization transfer schemes, and through selective inversion of protons combined with use of short relaxation times (Lundstrom and Akke, 2005; Schlagnitweit et al., 2018).

In the SELOPE experiment, imino protons are selectively excited and the magnetization belonging to non-imino protons is dephased prior to application of the B_1 field. This helps to suppress cross-relaxation (Yamazaki et al., 1994) between the imino and non-imino protons (*vide infra*). In addition, because the Watson-Crick to Hoogsteen exchange is relatively fast with k_{ex} = ~500 – 8000 s^{-1} at 25 °C (Alvey et al., 2014), we could afford to use a relatively short relaxation delay of 100 ms which also helped minimize NOE effects (*vide infra*) (Lundstrom and Akke, 2005; Schlagnitweit et al., 2018).

We initially performed experiments to evaluate contributions from ^{1}H-^{1}H cross-relaxation to the imino ^{1}H CEST profiles. In canonical B-form DNA and A-form RNA duplexes (Fig. 2), G-H1 is in closest proximity to the partner base C-H4a (~2.4 Å, Fig. 3a), while T/U-H3 is in closest proximity to the partner A-H2 (~2.8 Å, Fig. 3a). Additional proximal protons include imino and H2 protons of neighboring residues (~3.5-3.6 Å, Fig. 3a). These short internuclear distances are reflected in the intensity of cross peaks in 2D [^{1}H, ^{1}H] NOESY spectra of nucleic acid duplexes (Fig. 3b and Fig. S1). Note that although the amino proton of G-H2a is in proximity (2.2 Å) to G-H1, while the amino proton of A-H6a is in proximity (2.4 Å) to the partner T-H3 (Fig. 3a), these amino protons are typically not observable in 1D ^{1}H

or 2D [^{1}H,^{1}H] NOESY spectra caused by intermediate exchange due to the restricted rotation around the C-NH_2 bond (Schnieders et al., 2019).

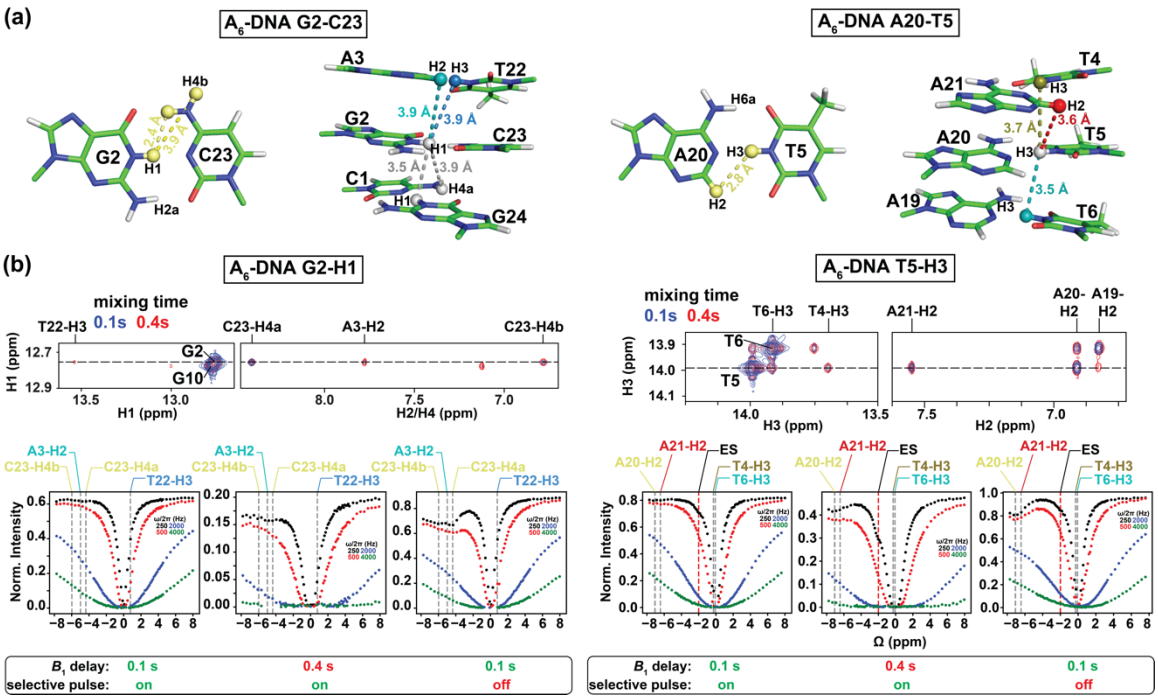

Figure 3. Analyzing NOE effects in ^{1}H CEST profiles. (a) Distances between the imino protons of G2-H1 and T5-H3 and nearby protons in the A_6-DNA duplex (PDBID: 5UZF). Note that although the amino proton of G-H2a is in proximity (2.2 Å) to G-H1, while the amino proton of A-H6a is in proximity (2.4 Å) to the partner T-H3, these amino protons are not observable in 1D ^{1}H or 2D [^{1}H,^{1}H] NOESY spectra caused by intermediate exchange due to the restricted rotation around the C-NH_2 bond (Schnieders et al., 2019). (b) NOE dips in ^{1}H CEST profiles for G2-H1 and T5-H3 in A_6-DNA. The NOE diagonal and cross peaks for G2-H and T5-

282 H3 in the 2D [^{1}H, ^{1}H] NOESY spectra with mixing time 100 ms (blue) and 400 ms
283 (red) are shown on the top. The ^{1}H CEST profiles for G2-H1 and T5-H3 with
284 combinations of short (100 ms) and long (400 ms) relaxation delays, with and
285 without selective excitation (Methods) are shown at the bottom. The ES frequency
286 (black) obtained from fitting ^{1}H CEST profiles with selective excitation and short
287 relaxation delay (100 ms) as well as frequency positions corresponding to the NOE
288 cross peaks in the 2D [^{1}H, ^{1}H] NOESY spectra (top) are highlighted according to
289 the color scheme in (a) (bottom). Error bars for CEST profiles in (b), which are
290 smaller than the data points, were obtained using triplicate experiments, as
291 described in Methods. RF powers for CEST profiles are color-coded.
292
293 ^{1}H CEST profiles (Fig. 3b and Fig. S2) for well-resolved imino resonances of A_6-
294 DNA (Fig. 2) were acquired simultaneously in a 1D manner using ~3 hours of
295 acquisition time on a spectrometer operating at 600 MHz ^{1}H frequency equipped
296 with a cryogenic probe, and using ~1.0 mM unlabeled DNA (Methods). Data were
297 initially collected at pH = 6.8. Under these near neutral pH conditions, it is
298 generally not feasible to detect the Watson-Crick to Hoogsteen exchange process
299 for G-C bps due to the low population of the protonated G-C$^+$ Hoogsteen bp
300 (Nikolova et al., 2013a). The lack of expected dips for the ES G-C$^+$ Hoogsteen bp
301 under these conditions provides an opportunity to better assess any extraneous

^{1}H CEST dips arising due to NOE effects. Unlike for G-C bps, the Hoogsteen exchange should still be detectable for A-T bps under these pH conditions.

Shown in Fig. 3b is a representative imino ^{1}H CEST profile measured for G2-H1 in the well-characterized A_6-DNA duplex (Nikolova et al., 2011). Besides the major dip, no additional dips were visible in the ^{1}H CEST profile. The major dip was also symmetric (Rangadurai et al., 2020a), indicating little to no contribution from Hoogsteen exchange or NOE effects, as expected for G-C bps under these pH conditions (Nikolova et al., 2013a). On the other hand, a minor shoulder was observed in the ^{1}H CEST profile of T5-H3 (Fig. 3b, the $\Delta\omega$ is highlighted by a dashed red line and labeled "ES"). The shoulder occurs at an offset frequency that does not correspond with any other observable proton frequency in the A_6-DNA duplex and is therefore unlikely to be the result of NOE effects (Fig. 3a). Rather, as will be described below, the shoulder corresponds to the ES Hoogsteen bp which is to be expected for the A-T bp at pH = 6.8.

To further verify that the dips observed in the ^{1}H CEST profile of T5-H3 and other thymine residues in A_6-DNA (see Fig. 4 and S2) do not represent an NOE effect, but rather reflect the ES Hoogsteen bp, we performed ^{1}H CEST experiments on a corresponding A_6-RNA duplex (Fig. 2). Unlike in B-form DNA duplexes, G-C$^+$ and

A-U Hoogsteen bps are both undetectable in A-form RNA duplexes by off-resonance ^{13}C and ^{15}N $R_{1\rho}$ RD, most likely due their much lower population (p_{ES} < 0.04 %) (Zhou et al., 2016; Rangadurai et al., 2018). If the shoulder observed in the ^{1}H CEST profile of T5-H3 in A_6-DNA is due to a Hoogsteen ES, and not NOE dips, we would expect to observe a symmetric profile without ES dips for U5-H3 in A_6-RNA. Indeed, the corresponding ^{1}H CEST profiles for U5-H3 (Fig. 4) and all other uridine and guanine (Fig. S3) imino protons in A_6-RNA were symmetric, with no evidence for any asymmetry or shoulder, indicating the absence of exchange and NOE effects.

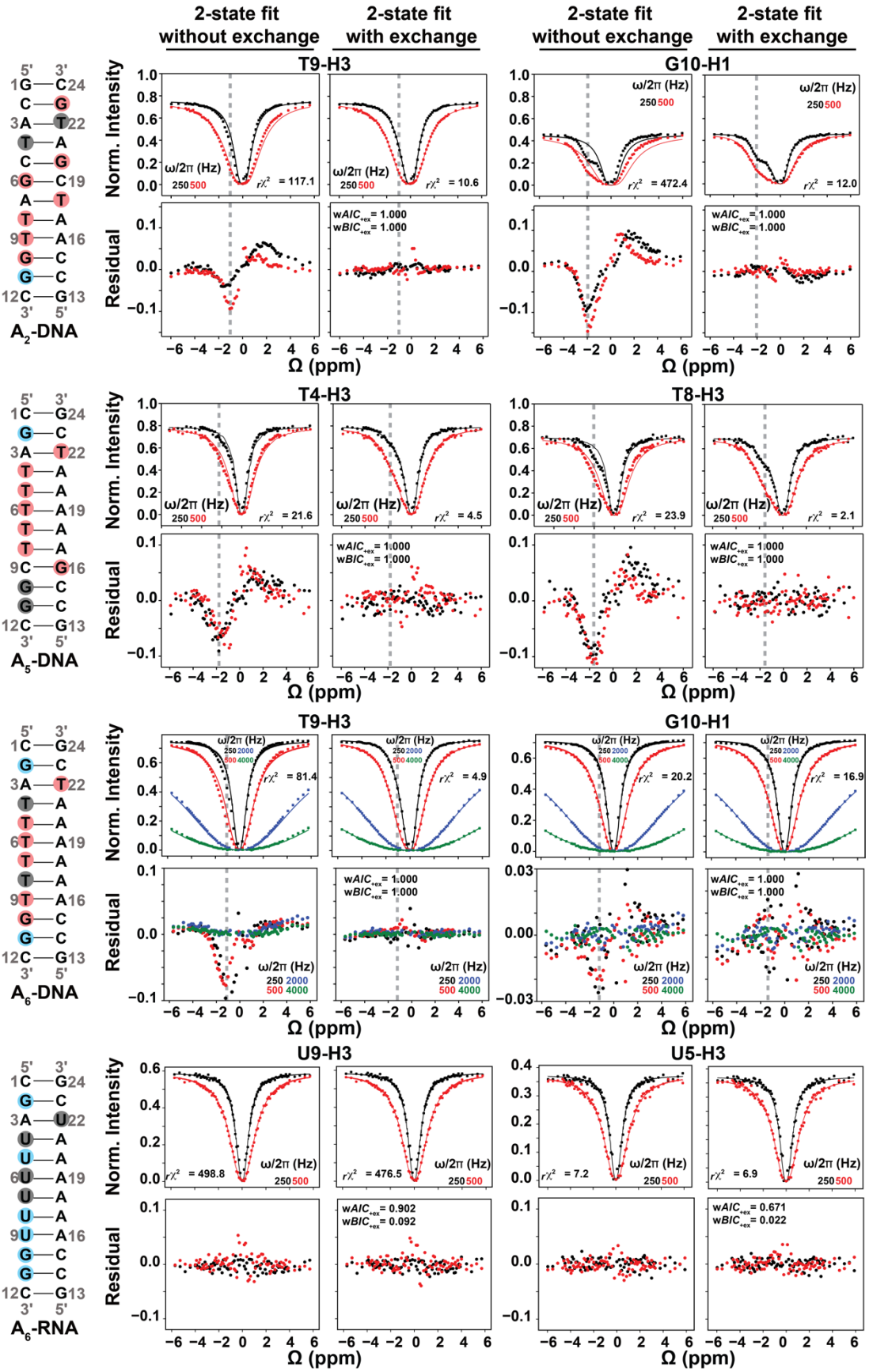
2-state fit without exchange
2-state fit with exchange
2-state fit without exchange
2-state fit with exchange
T9-H3
G10-H1
T4-H3
T8-H3
T9-H3
G10-H1
U9-H3
U5-H3
Norm. Intensity
Residual
Ω (ppm)
A2-DNA
A5-DNA
A6-DNA
A6-RNA
ω/2π (Hz)
250 500
250 2000 500 4000
rχ2 = 117.1
rχ2 = 10.6
rχ2 = 472.4
rχ2 = 12.0
rχ2 = 21.6
rχ2 = 4.5
rχ2 = 23.9
rχ2 = 2.1
rχ2 = 81.4
rχ2 = 4.9
rχ2 = 20.2
rχ2 = 16.9
rχ2 = 498.8
rχ2 = 476.5
rχ2 = 7.2
rχ2 = 6.9
wAIC+ex = 1.000
wBIC+ex = 1.000
wAIC+ex = 0.902
wBIC+ex = 0.092
wAIC+ex = 0.671
wBIC+ex = 0.022

332

Figure 4. Representative ^{1}H CEST profiles measured for A_2-DNA (pH 5.4) at 25 °C, A_5-DNA (pH 5.2) at 26 °C, A_6-DNA (pH 6.8) at 25 °C and A_6-RNA (pH 6.8) at 25 °C. Residues with detectable RD, undetectable RD, and overlapped 1D ^{1}H resonances (see Fig. 2) are highlighted in red, blue, and gray circles respectively. Shown are the fits of the ^{1}H CEST data to a 2-state Bloch-McConnell equation with and without (k_{ex} = Δω = p_{ES} = 0) chemical exchange. Shown below the CEST profiles are residual (experimental normalized intensity - fitted normalized intensity) plots. Also shown in inset are the reduced chi-square ($r\chi^2$), and Akaike's (w*AIC*) and Bayesian information criterion (w*BIC*) weights for fits with exchange (Methods). The dashed gray lines indicate the Hoogsteen Δω positions in both ^{1}H CEST profiles and in residual plots. Error bars for CEST profiles, which are smaller than the data points, were obtained using triplicate experiments, as described in Methods. RF powers for CEST profiles are color-coded.

Therefore, the shoulders in the ^{1}H CEST profiles (Fig. 3,4, Fig. S2,3) most likely rise due to chemical exchange with an ES. This was further confirmed by evaluating whether fits to the ^{1}H CEST profiles show any statistically significant improvement with the inclusion of exchange, as described below. Based on a similar analysis, no NOE dips were observable in the ^{1}H CEST profiles (Fig. 4, S2,3) for all other residues in A_6-DNA, A_6-RNA, and in two other DNA duplexes

across a range of pH and temperature conditions when using selective excitation and relaxation delay of 100 ms (Fig. 2, Fig. 4, and S2,3). These results indicate that any NOE effects between imino and non-imino protons are small under these experimental conditions.

Upon increasing the relaxation delay to 400 ms or using a non-selective ^{1}H excitation pulse (pulse **a** in Fig. 1b) with a delay of 100 ms, NOE dips became visible in the ^{1}H CEST profiles as shown for G2-H1 and T5-H3 (Fig. 3b) in A_6-DNA. The dips occurred at the ^{1}H resonance frequency of nearby protons, and as expected, were particularly pronounced for the partner C-H4a in the case of G2-H1 and the partner A-H2 in the case of T5-H3 (Fig. 3b). Nevertheless, even the ^{1}H CEST profiles acquired with 400 ms delay could be fit when restricting the offset to the imino proton region (-3 - 3 ppm), and the fitted exchange parameters were similar to those obtained from fitting profiles with 100 ms relaxation delay in which no NOE dips were visible (Fig. S4, Table S1). In contrast, the ^{1}H CEST profiles measured using non-selective excitation, which had larger NOE dips relative to using a selective excitation pulse, could not be satisfactorily fit (Fig. S4).

No NOE dips were observed at the chemical shift of imino protons belonging to neighboring residues in ^{1}H CEST profiles measured in DNA and RNA duplexes,

and none of the ^{1}H CEST profiles collected in thus study yielded an ES with Δω compatible with the imino ^{1}H chemical shift of a neighboring residue. Nevertheless, these NOE effects could be more difficult to assess given that they would be buried within the major dip. While imino-imino ^{1}H NOEs are not suppressed by selective excitation, their contribution is expected to be smaller relative to other NOE dips observed when using non-selective excitation (distances ~2.4 – 2.8 Å between guanosine/thymine imino and cytosine amino/adenine H2) due the larger distance of separation between neighboring imino protons (~3.5 – 3.9 Å) (Fig. 3a).

To further assess the impact of imino-imino ^{1}H NOEs on the ^{1}H CEST profiles, we examined whether selective excitation of imino protons (but not their immediate neighbors) results in different ^{1}H CEST profiles relative to an experiment in which all imino protons are excited. We performed an experiment selectively exciting G10-H1 and G2-H1 in A_6-DNA without exciting the imino resonances belonging to either of their two immediate neighbors. Selective excitation of individual imino protons resulted in ^{1}H CEST profiles (Fig. S2) and fitted parameters (Table S1) for G10-H1 and G2-H1 that are within error to those obtained when exciting all imino protons, again indicating that any imino-imino NOE contribution is negligible. Finally, the impact of imino-imino NOEs on the determination of the exchange

parameters was also assessed (*vida infra*) through comparison of the exchange parameters derived from fitting the imino ^{1}H CEST profiles with those measured independently using off-resonance ^{13}C and ^{15}N $R_{1\rho}$ RD measurements.

These results underscore the importance of critically evaluating the NOE contributions on a case-by-case basis (Schlagnitweit et al., 2018) and also suggest that NOE effects can be effectively suppressed for the canonical duplexes used in this study provided use of selective excitation and short relaxation delays.

It should be noted that to avoid any complexities due to NOE effects with water protons or hydrogen exchange, we restricted the offset to -6 ppm to 6 ppm when analyzing and fitting the ^{1}H CEST profiles. This is common practice as relatively narrow offsets (< 4 ppm) were used in prior ^{1}H CEST studies of both nucleic acids (Dubini et al., 2020; Wang et al., 2021; Liu et al., 2020) and proteins (Yuwen et al., 2017a; Yuwen et al., 2017b). While we did not observe a dip near the water chemical shift in the ^{1}H CEST profile for the internal residue T5-H3, a weak and broad dip near the water chemical shift was observed in the profile for the near terminal residue G2-H1 (Fig. S2). The latter dip could be due to NOEs between G2-H1 and water protons and/or due to fast hydrogen exchange kinetics.

2.2 Benchmarking the utility of ^{1}H CEST to probe Watson-Crick to Hoogsteen exchange in DNA duplexes

To examine the utility of the SELOPE ^{1}H CEST experiment to characterize Watson-Crick to Hoogsteen exchange, we benchmarked the experiment by measuring conformational exchange in three DNA duplexes (A_6-DNA, A_2-DNA and A_5-DNA, Fig. 2) for which we have previously extensively characterized the Watson-Crick to Hoogsteen exchange using ^{13}C and ^{15}N off-resonance $R_{1\rho}$ (Nikolova et al., 2011; Alvey et al., 2014; Shi et al., 2018) and CEST (Rangadurai et al., 2020a; Rangadurai et al., 2020b) experiments. We compared the exchange parameters derived using ^{1}H CEST with counterparts derived using ^{13}C/^{15}N $R_{1\rho}$ or CEST for a variety of G-C and A-T bps across three different DNA duplexes and varying pH (5.2-6.8) conditions. All ^{1}H CEST experiments were performed using 100 ms relaxation delay and selective excitation.

As expected, for several thymine residues, the imino ^{1}H CEST profile was visibly asymmetric (Fig. 4 and Fig. S2,3), consistent with relatively fast (k_{ex} > 1000 s^{-1}) Watson-Crick to Hoogsteen exchange. The asymmetry manifests as an upfield shifted shoulder (e.g. T8-H3 in A_5-DNA in Fig. 4) as expected for T-H3 Hoogsteen chemical shift ($\Delta\omega$ ~-2 ppm) (Nikolova et al., 2011; Xu et al., 2018). In other cases, such as T9-H3 in A_6-DNA, the asymmetry was less pronounced, and the exchange

433 contribution was only apparent following comparison of fits with and without
434 exchange (see Fig. 4).
435
436 As expected, at pH = 6.8, the imino ^{1}H CEST profiles were symmetric for most
437 guanine residues consistent with no observable exchange (Fig. 4 and S2,3).
438 However, the major dip became asymmetric for several guanine residues when
439 lowering the pH to 5.2 or 5.4, as expected for the Watson-Crick to Hoogsteen
440 exchange of G-C bps, which is favored at lower pH (Fig. 4 and S3). All minor dips
441 occurred at resonance frequencies that did not correspond with any other protons
442 in the molecule (Fig. 2 and S1,2). In all cases, the ^{1}H CEST profiles could be
443 satisfactorily fit to a 2-state model with or without exchange, suggesting that any
444 NOE contribution to the ^{1}H CEST profile is likely to be insignificant.
445
446 To identify which imino ^{1}H CEST profiles have significant chemical exchange
447 contributions, each profile was subjected to a fit with or without ($\Delta\omega = p_{ES} = k_{ex} =$
448 0) 2-state chemical exchange (Methods). Akaike information criterion (AIC) and
449 Bayesian information criterion (BIC) (Burnham and Anderson, 2004) weights were
450 then used to evaluate whether any improvement in the fit due to inclusion of
451 chemical exchange was statistically significant (Kimsey et al., 2018; Liu et al.,
452 2020). The improvement of fit was considered to be statistically significant when

both AIC and BIC weights > 0.995 and the reduced chi-square ($r\chi^2$) is reduced with the inclusion of exchange. Residual plots were also used to visualize changes in fit quality (Fig. 4).

Based on the AIC and BIC analysis, all thymine and guanine residues shown previously to undergo Watson-Crick to Hoogsteen exchange using off-resonance ^{13}C and/or ^{15}N $R_{1\rho}$ under these experimental conditions, also showed statistically significant improvements when fitting the ^{1}H CEST profiles with the inclusion of chemical exchange (Fig. 4 and S2,3). On the other hand, all guanine residues including G2 and G11 in A_6-DNA and G11 in A_2-DNA, which did not show signs of Hoogsteen exchange in off-resonance ^{13}C and/or ^{15}N $R_{1\rho}$ (Nikolova et al., 2011; Shi et al., 2018) under these experimental conditions also did not show statistically significant improvements when fitting their ^{1}H CEST profiles with the inclusion of chemical exchange (Fig. 4 and S2,3).

Interestingly, a few residues including T5, T6, T7 and T22 in A_6-DNA, T18, G6 and G20 in A_2-DNA (Fig. S2,3), showed exchange based on ^{1}H CEST but did not show evidence for Hoogsteen exchange based on prior off-resonance ^{13}C and/or ^{15}N $R_{1\rho}$ experiments (Nikolova et al., 2011; Alvey et al., 2014; Shi et al., 2018). As will be elaborated in the following section, these data provide new insights into the

473 Watson-Crick to Hoogsteen exchange process, and suggest that at least in some
474 cases, ^{1}H CEST can exceed the detection limits of ^{13}C/^{15}N based methods.
475
476 In addition, T18 and G20 in A_2-DNA were difficult to probe using ^{13}C RD due to
477 spectra overlap (Nikolova et al., 2011) but could easily be measured using ^{1}H
478 CEST (Fig. 2, 4 and S3). In contrast, other residues such as T8 and T4 in A_6-DNA,
479 T4 and T22 in A_2-DNA, and G10 and G11 in A_5-DNA could be targeted for ^{13}C or
480 ^{15}N RD measurements (Nikolova et al., 2011; Alvey et al., 2014) but could not be
481 measured by ^{1}H CEST due to overlap in the 1D ^{1}H imino spectra (Fig. 2). This
482 highlights the complementarity of ^{1}H and ^{13}C/^{15}N RD in characterizing Watson-
483 Crick to Hoogsteen exchange.
484
485 To assess how well the exchange parameters are determined by the ^{1}H CEST
486 data, we subjected the ^{1}H CEST profiles for residues T7 ($k_{ex}/\Delta\omega \sim 0.2$), T9 ($k_{ex}/\Delta\omega$
487 ~ 0.82) and T22 ($k_{ex}/\Delta\omega \sim 3.5$) which exhibit exchange on the slow, intermediate,
488 and fast timescale (Rangadurai et al., 2019b) respectively, to a degeneracy
489 analysis. We computed the reduced chi-square ($r\chi^2$) for a 2-state fit as a function
490 of varying k_{ex}, $\Delta\omega$ or p_{ES}. In all cases, the $r\chi^2$ values increased significantly (up
491 to 10-fold) when varying k_{ex}, $\Delta\omega$ or p_{ES} by 3-fold (Fig. S5), indicating that the
492 exchange parameters are well-defined by the ^{1}H CEST data.

To test the accuracy of the exchange parameters obtained using ^{1}H CEST, we compared the exchange parameters p_{ES} and k_{ex}, derived from a 2-state fit of the data to values determined previously using off-resonance ^{13}C and/or ^{15}N $R_{1\rho}$ (Nikolova et al., 2011; Shi et al., 2018; Alvey et al., 2014) for Hoogsteen dynamics (Fig. 5a and Table S1). In total, we were able to compare 13 data points from ^{1}H CEST and ^{13}C/^{15}N $R_{1\rho}$ for three different duplexes under different conditions of temperature and pH (Fig. 2,5a). This comparison also allowed us to further verify that the exchange process detected by ^{1}H CEST does indeed correspond Watson-Crick to Hoogsteen exchange, and to also further assess for potential contributions from NOE effects, which might cause deviations from agreement.

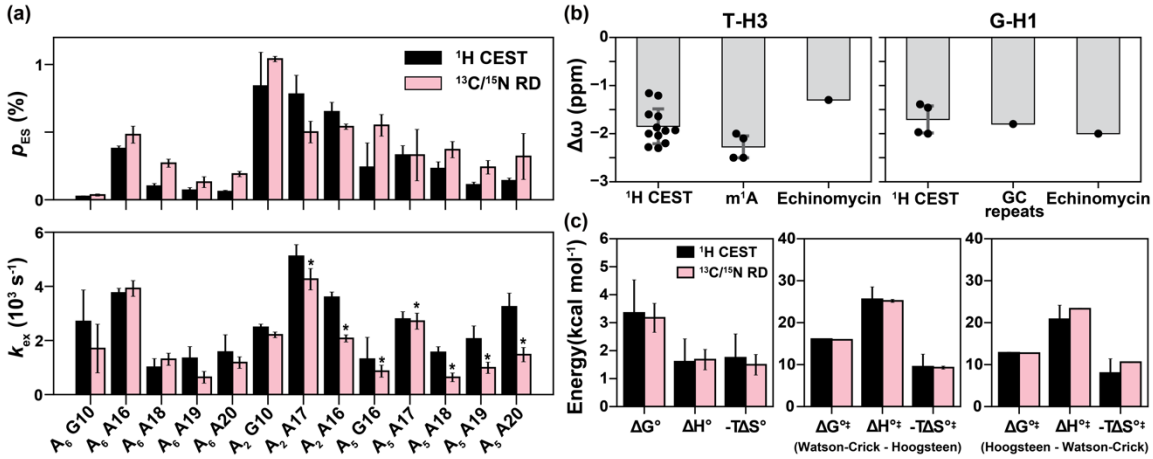

Figure 5. Comparison of exchange parameters for the Watson-Crick to Hoogsteen exchange obtained from ^{1}H CEST and ^{13}C/^{15}N $R_{1\rho}$. (a) Comparison of

exchange parameters (k_{ex} and p_{ES}) measured using ^{1}H CEST with counterparts previously reported using ^{13}C/^{15}N off-resonance $R_{1\rho}$ (Nikolova et al., 2011; Alvey et al., 2014; Shi et al., 2018). ^{13}C RD data for A18, A19 and A20 were measured using off-resonance $R_{1\rho}$ in this study (Fig. S7). Small systematic deviations in k_{ex} for the values indicated with asterisks could be due to small differences in temperature (< 0.8ºC) across different spectrometers. Bps are specified by the corresponding purine residue. (b) Comparison of the Δω obtained from fitting ^{1}H CEST profiles for T-H3 and G-H1 (Table S1) with the values expected for a Watson-Crick to Hoogsteen transition based on duplexes in which A-T or G-C^{+} Hoogsteen bps were rendered the dominant state, by using N^{1}-methylated adenine ($m^{1}A$) (Nikolova et al., 2011; Sathyamoorthy et al., 2017; Rangadurai et al., 2020b), by binding of the drug (echinomycin) to a DNA duplex (Xu et al., 2018), or through use of GC repeat sequences (GC repeats) that predominantly form Hoogsteen bps at low pH (Stelling et al., 2017). (c) Comparison of free energy (ΔG°), enthalpy (ΔH°) and entropy (-TΔS°, T = 25 °C) of the Watson-Crick to Hoogsteen transition, and the activation free energy (ΔG°‡), enthalpy (ΔH°‡) and entropy (-TΔS°‡, T = 25 °C) for Watson-Crick to Hoogsteen (Watson-Crick - Hoogsteen) and Hoogsteen to Watson-Crick (Hoogsteen - Watson-Crick) transitions measured using ^{1}H CEST in this study and using ^{13}C $R_{1\rho}$ from Nikolova *et al* (Nikolova et al., 2011). The energetics in (c) were measured for the Watson-

528 Crick to Hoogsteen transition of A16-T9 in A_6-DNA at pH 6.8. Errors in (a) were
529 fitting errors of ^{1}H CEST, calculated as described in Methods or errors of ^{13}C/^{15}N
530 $R_{1\rho}$ calculated using a Monte-Carlo scheme as described previously (Rangadurai
531 et al., 2019b). Errors in (b) are the standard deviations of data points (shown as
532 black dots) in each category. Error bars in (c) were propagated from the errors in
533 the exchange parameters obtained from ^{1}H CEST or ^{13}C/^{15}N $R_{1\rho}$.
534
535
536 Indeed, the p_{ES} and k_{ex} values derived using ^{1}H CEST were in very good
537 agreement with their off-resonance ^{13}C and/or ^{15}N $R_{1\rho}$ counterparts (Fig. 5a). The
538 differences between k_{ex} and p_{ES} measured using the two methods was often within
539 error with the largest differences being <3-fold. A small and systematic difference
540 in k_{ex} was observed for a subset of the data (Fig. 5a), and this might be due to
541 small temperature differences (<0.8ºC) between spectrometers. Importantly, the
542 ES imino ^{1}H chemical shifts deduced from a 2-state fit of the ^{1}H CEST profiles
543 ($\Delta\omega_{A\text{-}T}$ = ~-1 to -2 ppm and $\Delta\omega_{G\text{-}C}$ = ~-1.5 to -2.0 ppm) were also in good agreement
544 with the expected range of values ($\Delta\omega$ = -1 to -2 ppm) for Hoogsteen bps (Fig. 5b)
545 based on studies of duplexes containing Hoogsteen bps as the dominant
546 conformation (Nikolova et al., 2011; Stelling et al., 2017; Xu et al., 2018;
547 Rangadurai et al., 2020b).

As an additional test, we also measured temperature-dependent (5 °C, 10 °C, 20 °C, 25 °C, 30 °C and 45 °C) ^{1}H CEST profiles for A_6-DNA at pH 6.8 (Fig. S2), and then used the temperature dependence of the fitted kinetic rate constants (k_1 and k_{-1}) to determine the standard and activation enthalpy and entropy changes for the Watson-Crick to Hoogsteen transition (Fig. S6). These values were in excellent agreement with those measured from off-resonance ^{13}C $R_{1\rho}$ (Nikolova et al., 2011) (Fig. 5c), further supporting the robustness of the ^{1}H CEST methodology.

2.3 New insights into Hoogsteen breathing

^{1}H CEST profiles for some residues show detectable exchange contributions when corresponding ^{13}C/^{15}N RD measurements do not or show only weak exchange. This suggests that ^{1}H CEST can provide additional insights into Watson-Crick to Hoogsteen exchange and extend the detection limits of conventional ^{13}C/^{15}N RD measurements.

For example, using ^{1}H CEST it was feasible to measure Watson-Crick to Hoogsteen exchange for T5-H3, T6-H3, and T7-H3 (Fig. S2) within the middle of the A-tract motif (defined as A_n-tract with n>3) in A_6-DNA. These residues had

previously exhibited only weak on-resonance ^{13}C $R_{1\rho}$ RD, and as a result, no off-resonance $R_{1\rho}$ data were ever recorded (Nikolova et al., 2011). Based on the ^{1}H CEST measurements, residues within the A-tract motif have ten-fold lower Hoogsteen population (p_{ES} = 0.06±0.01 %-0.09±0.03 %) relative to other A-T bps in A_6-DNA (p_{ES} > ~0.10 %) (Table S1). These represent the lowest A-T Hoogsteen populations ever recorded to date in duplex DNA (Table S1). The exchange kinetics were also 2-fold slower (k_{ex} ~1000 s^{-1}) for the A-tract residues relative to other A-T bps (k_{ex} > 2000 s^{-1}) in A_6-DNA (Table S1). Interestingly, the suppression of Hoogsteen dynamics within the A-tract motif appears to be A-tract length dependent, with both the Hoogteen population and exchange kinetics increasing slightly for similar bps in A_5-DNA (Table S1). The suppression of Hoogsteen dynamics within A-tracts is consistent with prior studies showing them to be more rigid and stiff motifs relative to scrambled DNA (Nikolova et al., 2012b). We verified these ^{1}H CEST derived exchange parameters for A-tract residues in A_6-DNA by performing off-resonance ^{13}C $R_{1\rho}$ measurements (Fig. S7) on uniformly $^{13}C/^{15}N$ labeled A_6-DNA and did indeed observe the expected RD with p_{ES} and k_{ex} values similar (difference <3-fold, Fig. 5a) to those measured using ^{1}H CEST. These prospective tests of the ^{1}H CEST data using off-resonance $^{13}C/^{15}N$ $R_{1\rho}$ RD data further support the methodology.

587 The ability to characterize fast exchange kinetics has long been a motivation for
588 using ^{1}H in RD experiments to characterize conformational exchange (Ishima et
589 al., 1998; Ishima and Torchia, 2003; Eichmuller and Skrynnikov, 2005; Lundstrom
590 and Akke, 2005; Otten et al., 2010; Hansen et al., 2012; Smith et al., 2015; Steiner
591 et al., 2016; Furukawa et al., 2021). Indeed, ^{1}H CEST made it possible to measure
592 fast Watson-Crick to Hoogsteen exchange kinetics which were undetectable by
593 off-resonance ^{13}C $R_{1\rho}$. In particular, it was possible to measure Watson-Crick to
594 Hoogsteen exchange for T22 in A_6-DNA with k_{ex} > 20,000 s^{-1} (Fig. S2 and Table
595 S1), which is the fastest ever recorded Hoogsteen exchange process at 25 °C
596 (Table S1). In contrast, the off-resonance ^{13}C $R_{1\rho}$ RD profiles reported for this
597 residue in prior studies were flat (Nikolova et al., 2011; Shi et al., 2018), and
598 simulations show that such an exchange process is too fast for reliable detection
599 using ^{13}C $R_{1\rho}$ (Fig. S8a). Similarly, it was feasible to measure Watson-Crick to
600 Hoogsteen exchange for G6 (p_{ES} ~0.3 %, k_{ex} ~3000 s^{-1}) in A_2-DNA using ^{1}H CEST
601 yet no off-resonance ^{13}C $R_{1\rho}$ RD on C1' was previously detected (Shi et al., 2018),
602 which based on simulations, was likely due to a combination of exchange kinetics
603 and small Δω value (Fig. S8b).
604
605 One of the potential utilities of the ^{1}H CEST experiment is the measurement of very
606 fast exchange kinetics at high temperatures and in a manner insensitive to melting

607 of duplexes, shown previously to complicate analysis of Hoogsteen exchange
608 using ^{13}C and ^{15}N RD (Shi et al., 2019). Melting of duplexes should not yield any
609 exchange dips around the imino ^{1}H region given that the imino protons of single-
610 stranded species (ssDNA) exchange rapidly with solvent.
611
612 We therefore measured ^{1}H CEST profiles for A_6-DNA at 45 °C (Fig. S2), in which
613 the ssDNA population is ~10 % (Shi et al., 2019). We did not observe any evidence
614 for the ssDNA species in the ^{1}H CEST profiles. Instead, we were able to observe
615 ultra-fast (k_{ex} ~ 10,000 s^{-1}, see Table S1) Hoogsteen exchange which could not
616 previously be detected by ^{13}C or ^{15}N RD experiments at the same temperature (Shi
617 et al., 2019).
618
619 Taken together, these results demonstrate that the ^{1}H CEST experiment broadens
620 the range of populations and exchange rates over which Hoogsteen breathing can
621 be effectively characterized.

622 **3 Discussion**

623 Building on prior studies showing the utility of the SELOPE ^{1}H RD experiment in
624 measuring conformational exchange in unlabeled RNA (Schlagnitweit et al., 2018)

and DNA (Furukawa et al., 2021; Dubini et al., 2020), our study establishes the utility of high-power ^{1}H CEST SELOPE as a facile means for rapidly assessing the Watson-Crick to Hoogsteen exchange process in nucleic acids without the need for isotopic enrichment. The methodology is supported by the very good agreement observed between the measured exchange parameters and values measured independently using ^{13}C and/or ^{15}N $R_{1\rho}$ for a variety of bps in three duplexes under different conditions of temperature and pH, as well as by the good agreement seen between the imino ^{1}H chemical shifts and those expected based on duplexes containing Hoogsteen bps as the dominant GS conformation. The high throughput nature of the experiment and simple sample requirements enabled us to measure Hoogsteen dynamics for 37 data points corresponding to 22 distinct bps for three different pH conditions and seven different temperatures (Table S1), the largest collection of Hoogsteen dynamics from a single study to date. We envision using the ^{1}H CEST SELOPE experiments to pre-screen DNA duplexes and to perform follow-up ^{13}C and ^{15}N RD experiments to confirm any interesting outliers, particularly regions showing substantially elevated Hoogsteen dynamics.

An important consideration when applying ^{1}H CEST to the study of chemical exchange are contributions due to ^{1}H-^{1}H cross-relaxation originating from cross relaxation, which may give rise to extraneous NOE dips that complicate data

analysis (Yuwen et al., 2017a; Bouvignies and Kay, 2012; Eichmuller and Skrynnikov, 2005). These contributions have been shown to be significant in proteins particularly when characterizing slow exchange (k_{ex} < 200 s^{-1}) necessitating use of relatively long relaxation delays (Bouvignies and Kay, 2012). Consistent with prior studies of nucleic acids (Schlagnitweit et al., 2018; Steiner et al., 2016; Baronti et al., 2020) and proteins (Lundstrom and Akke, 2005). Our results indicate that NOE effects from cross-relaxation between imino and non-imino protons can be effectively suppressed for DNA and RNA duplexes in the ^{1}H CEST experiments through selective excitation provided that the relaxation delays are short on the order of 100 ms (Fig. 3b). However, care should be exercised to assess imino-imino NOE effects (Fig. 3b), which may also be more substantial for certain non-canonical motifs. Data should be discarded if the ES chemical shifts match those of nearby imino protons identified using 2D [^{1}H, ^{1}H] NOESY experiments or if the magnitude of the dip of interest varies substantially with or without selective excitation, as this could be an indication of NOE effect. Finally, we recommend independent verification of the exchange parameters with the use of other methods such as ^{13}C and ^{15}N experiments for motifs exhibiting highly unusual exchange parameters or ES ^{1}H chemical shifts, and this can also help to confirm Hoogsteen bps as the ES.

665 Prior studies showed that Watson-Crick to Hoogsteen bp transitions exhibit large
666 variations in the forward rate constants (k_1) while the backward rate constants (k_{-1})
667 is relatively constant across different sequence contexts, consistent with a late
668 transitional state (Alvey et al., 2014). We observe a similar trend in which k_{-1} varied
669 <5-fold while k_1 varied by ~50-fold (Fig. S9). The ^{1}H CEST data also revealed
670 significantly lower Hoogsteen abundance (p_{ES} < 0.1 %) in addition to slower
671 exchange kinetics (k_{ex} ~1,000 s^{-1}) within A-tract motifs (Nikolova et al., 2011; Alvey
672 et al., 2014), while also reinforcing prior data (Xu et al., 2018) suggesting increased
673 exchange kinetics near terminal ends. Collectively, these data show that the
674 Hoogsteen population can vary by as much as ~14-fold while k_{ex} can vary by ~20-
675 fold only due to changes in sequence and positional context (Table S1). These
676 strong sequence and position dependencies could play important roles in
677 biochemical processes acting on DNA.
678
679 A recent study (Furukawa et al., 2021) reported on-resonance imino ^{1}H $R_{1\rho}$ RD for
680 a guanine residue in a DNA duplex at pH = 7.5, T= 30 °C, and in 150 mM NaCl.
681 Because off-resonance measurements were not performed, only k_{ex} ~ 10,000 s^{-1}
682 could be determined while the values of Δω and p_{ES} were not determined. The
683 study noted that a Hoogsteen bp as the ES was unlikely given that G-C$^+$ Hoogsteen
684 bps are disfavored at pH= 7.5 and because the observed rate of exchange (k_{ex} ~

685 10,000 s^{-1}) was much faster than is typically observed for Watson-Crick to
686 Hoogsteen exchange. Instead, the data were interpreted as evidence for a base
687 opened state. However, the observed rate of exchange k_{ex} ~10,000 s^{-1} falls
688 comfortably within the range of values measured here for Watson-Crick to
689 Hoogsteen exchange using ^{1}H CEST at similar pH conditions. For example, for
690 the G10-C15 bp in A_6-DNA at the same temperature and pH = 6.8, k_{ex} for Watson-
691 Crick to Hoogsteen exchange was ~6,000 s^{-1} (Fig. 4 and Table S1). Similar
692 Watson-Crick to Hoogsteen exchange parameters (p_{ES} ~0.05 % and k_{ex} ~2000 s^{-1}
693) were recently reported for this bp at 25 °C and pH 6.8 using cytosine amino ^{15}N
694 RD (Rangadurai et al., 2019a) and the ES $\Delta\omega_{C\text{-}N4}$ = -9 ppm was shown to be in
695 excellent agreement with values expected for a G-C^{+} Hoogsteen bp. In addition,
696 based on hydrogen exchange measurements, p_{ES} ~0.00001 % to 0.01 % and k_{ex}
697 (k_{cl} + k_{op}, k_{cl} and k_{op} are the base closing and opening rate constant, respectively)
698 ~ 10^5 to 10^7 s^{-1} for the base-opened ES, and this process should fall outside RD
699 detection (Gueron and Leroy, 1995; Gueron et al., 1987; Leroy et al., 1988; Leijon
700 and Graslund, 1992; Snoussi and Leroy, 2001). Therefore, the ES detected by
701 Furukawa *et al* (Furukawa et al., 2021) is more likely a Hoogsteen bp.
702
703 In conclusion, by obviating the need for isotopic enrichment, the ^{1}H CEST
704 experiment expands the scope of characterizing Watson-Crick to Hoogsteen

exchange in nucleic acids by NMR. We are presently applying the experiment to map the sequence dependence of Hoogsteen breathing dynamics and systematically, how it varies with pH, salt, and crowding, and following the introduction of lesions, mismatches, and molecules that bind to the DNA.

4 Methods

4.1 Sample preparation

Unlabeled DNA and RNA oligonucleotides: Unmodified DNA oligonucleotides were purchased from Integrated DNA Technologies with standard desalting purification. RNA oligonucleotides were synthesized using a MerMade 6 Oligo Synthesizer employing 2'-tBDSilyl protected phosphoramidites (n-acetyl protected rC, rA and rG, and rU phosphoramidites were purchased from Chemgenes) and 1 µmol standard synthesis columns (1000 Å) (BioAutomation). RNA oligonucleotides were synthesized with the final 5'-protecting group, 4,4'-dimethoxytrityl (DMT) retained. RNA oligonucleotides were cleaved from columns using 1 ml AMA (1:1 ratio of 30 % ammonium hydroxide and 30 % methylamine) and incubated at room temperature for 2 hours. The sample was then air-dried and dissolved in 115 µL DMSO, 60 µL TEA, and 75uL TEA.3HF, and then incubated at T = 65 °C for 2.5 hours to remove 2'-O protecting groups. The Glen-Pak RNA cartridges (Glen Research Corporation) were then used to purify the samples followed by ethanol precipitation.

Labeled DNA oligonucleotides: The uniformly ^{13}C, ^{15}N labeled A_6-DNA sample was prepared using chemically synthesized DNA (purchased from IDT), Klenow

fragment DNA polymerase (New England Biolab) and $^{13}C/^{15}N$ isotopically labeled dNTPs (Silantes) using the Zimmer and Crothers method (Zimmer and Crothers, 1995). The oligonucleotide was purified using 20 % 29:1 polyacrylamide denaturing gel with 8 M urea, 20 mM Tris borate and 1 mM EDTA, and then using electro-elution (Whatmann, GE Healthcare) in 40 mM Tris Acetate and 1 mM EDTA, followed by ethanol precipitation.

Sample annealing and buffer exchange: DNA/RNA oligonucleotides were re-suspended in water (200-500 μM). To prepare duplex samples, equimolar amounts of the constituent single stranded DNA/RNA samples were mixed and then heated at T = 95 °C for ~5 min followed by cooling at room temperature for ~1 hour. All samples were exchanged three times into the desired buffer using centrifugal concentrators (4 mL, Millipore Sigma). 10 % D_2O (Millipore Sigma) was added to the samples prior to the NMR measurements.

Sample concentrations and buffer conditions: Unless mentioned otherwise, the NMR buffer contains 25 mM sodium chloride, 15 mM sodium phosphate, 0.1 mM EDTA and 10 % D_2O. Sample concentrations and buffer pH: A_6-DNA, 1.0 mM, pH 6.8; A_2-DNA, 1.0 mM, pH 5.4; A_5-DNA, 0.2 mM, pH 5.2; A_6-RNA, 0.5 mM, pH 6.8. Concentration was estimated by measuring the absorbance of the sample at

260nm and using extinction coefficients from the ADT Biol Oligo calculator (https://www.atdbio.com/tools/oligo-calculator).

4.2 NMR spectroscopy

All NMR experiments were performed on a 600 BrukerAvance 3 spectrometer equipped with a triple-resonance HCN cryo-genic probe. The NMR data were processed and analyzed with NMRpipe (Delaglio et al., 1995) and SPARKY (T.D. Goddard and D.G. Kneller, SPARKY 3, University of California, San Francisco).

Resonance assignments: Imino resonances were assigned using a combination of 2D [^{1}H, ^{1}H] NOESY and [^{15}N,^{1}H] SOFAST-HMQC (Sathyamoorthy et al., 2014) experiments. Assignments for A_6-DNA, A_2-DNA and A_6-RNA were reported previously (Sathyamoorthy et al., 2017; Zhou et al., 2016; Nikolova et al., 2011). The [^{1}H, ^{1}H] NOESY spectrum for A_5-DNA is shown in Fig. S1.

^{1}H CEST: The pulse sequence was shown in Fig. 1b, and was adapted from Schlagnitweit *et al* (Schlagnitweit et al., 2018). The g1 gradient (Fig. 1b) destroys transverse ^{1}H magnetization prior to excitation of imino resonances. This helps to avoid any accidental offset dependence of the starting ^{1}H magnetization.

Relaxation delays T_{EX} = 100 ms was used for all ^{1}H CEST measurements at low temperatures (5 °C – 30 °C), while a shorter T_{EX} = 80 ms was used for high (45 °C) temperature measurements. A longer T_{EX} = 400 ms was used to illustrate artefacts arising due to NOE dips (Fig. 3b). RF power and offset combinations used in the CEST measurements are given in Table S2. Calibration of RF field powers for the ^{1}H CEST measurements was performed as described previously (Rangadurai et al., 2019b) using the same pulse sequence. Field inhomogeneity was also measured (Fig. S10) using the same sequence and the procedure as described previously (Guenneugues et al., 1999). ^{1}H inhomogeneity was measured by performing on-resonance ^{1}H CEST experiments on G2-H1 of A_6-DNA, chosen as it does not experience conformational exchange. The longest relaxation delay used for the measurements were 10 s, 2 s, 1 s, 0.4 s, 0.1 s and 0.04 s for RF fields 10 Hz, 50 Hz, 100 Hz, 200 Hz, 1000 Hz and 4000 Hz, respectively. The resulting nutation curve was Fourier transformed and was fit to a gaussian function (blue lines in Fig. S10) to extract the full-width at half-maximum, which was used for defining the inhomogeneity as described previously (Guenneugues et al., 1999). The selective pulse was set to be off (Fig. 3b) by replacing pulse **a** (Fig. 1b) with a non-selective ^{1}H hard 90° pulse. 16 scans were used for A_6-DNA (1.0 mM) at 5°C, 10°C, 20°C, 25°C, 30°C, and A_2-DNA (1.0 mM) at 25°C. 32 scans were used for

A_6-RNA (0.5 mM) at 25°C. 64 scans were used for A_5-DNA (0.2 mM) at 25°C and for A_6-DNA (1.0 mM) at 45°C.

Fitting of ^1H CEST data: When performing 2-state CEST fitting with and without exchange, we restricted the offset to -6 to 6 ppm for ^{1}H CEST experiment with relaxation delay $\leq$ 100 ms, and to -3 to 3 ppm for experiments with relaxation delay = 400 ms, to obviate any potential effects from ^{1}H-^{1}H cross-relaxation artifacts (Fig. 3b). Peak intensities of all imino protons in the 1D spectra as a function of RF power and offset frequency were extracted using NMRPipe (Delaglio et al., 1995). The peak intensity at a given RF power and offset is normalized by the average peak intensity over the triplicate CEST measurements with zero relaxation delay under the same RF power. The uncertainty in the measured peak intensity at each offset frequency and RF power combination was assumed to be equal to the standard deviation of the peak intensities for triplicate CEST experiments with zero relaxation delay under the same RF power (Zhao et al., 2014; Shi et al., 2019). CEST profiles were generated by plotting the normalized intensity as a function of offset $\Omega = \omega_{RF} - \omega_{obs}$ where ω_{obs} is the Larmor frequency of the observed resonance and ω_{RF} is the angular frequency of the applied RF field. RF field inhomogeneity (Fig. S10) was taken into account during CEST fitting as described previously (Rangadurai et al., 2020a). The normalized CEST profiles were then fit

via numerical integration of the Bloch-McConnell (B-M) equations as described previously (Rangadurai et al., 2020a). Fitting of CEST profiles without exchange (Fig. 4, Fig. S2-4) was performed by setting p_{ES} = k_{ex} = $\Delta\omega$ = 0. Errors in exchange parameters were set to be equal to the fitting errors which were obtained as the square root of the diagonal elements of the covariance matrix. Reduced chi-square ($r\chi^2$) was calculated to assess the goodness of fitting (Rangadurai et al., 2019b). Note that the variations in $r\chi^2$ values for different ^{1}H CEST profiles in Fig. 4 and Fig. S2-4 are most likely due to differences in the quality of the NMR data and poor estimation of the real experimental uncertainty. The residual sum of squares (RSS) was computed as follows

$$RSS = \sum_{i=1}^{n} \left(I_i^{fit} - I_i^{exp}\right)^2 \quad (1)$$

$where\ I_i^{fit}$ and I_i^{exp} are the *i*th fit and experimentally measured intensity in the CEST profile respectively, and the summation is over all RF power and offset combinations (N).

Model selection for fits with and without exchange (Fig. 4, Fig. S2-4) was performed by computing AIC and BIC weights as follows (Burnham and Anderson, 2004):

$$AIC = \begin{cases} Nln\left(\frac{RSS}{N}\right) + 2K, & when \frac{N}{K} \geq 40 \\ Nln\left(\frac{RSS}{N}\right) + 2K + \frac{2K(K+1)}{N-K-1}, & when \frac{N}{K} < 40 \end{cases} \quad (2)$$

$$wAIC = \frac{e^{-0.5\Delta AIC}}{1 + e^{-0.5\Delta AIC}} \quad (3)$$

$$BIC = Nln\left(\frac{RSS}{N}\right) + Kln(N) \quad (4)$$

$$wBIC = \frac{e^{-0.5\Delta BIC}}{1 + e^{-0.5\Delta BIC}} \quad (5)$$

Where *K* is the number of floating parameters when fitting and $\Delta AIC/\Delta BIC$ are the differences between two AIC values (fitting without and with exchange). The AIC ($wAIC_{+ex}$) and BIC ($wBIC_{+ex}$) weights for fits with exchange are reported in Fig. 4 and Fig. S2-4. The improvement in the fit was considered statistically significant if both $wAIC_{+ex}$ and $wBIC_{+ex}$ values are > 0.995, and $r\chi^2$ is reduced with the inclusion of exchange. For some resonances, the improvement in the fit with exchange are statistically significant but the resulting exchange parameters are not reliable and have large errors (see Fig. S2,3). For T4 in A_5-DNA, p_{ES} = 0.2±0.1 % measured using ^{1}H CEST was ~10-fold smaller than p_{ES} = 2.7±1.5 % measured previously using ^{15}N RD (Alvey et al., 2014), whereas k_{ex} (~3000 s^{-1}) was is in good agreement. However, simulations show that due to the small Δω for ^{15}N (~1 ppm)

844 and fast exchange kinetics k_{ex} (~3000 s^{-1}) the p_{ES} and Δω are not well-determined
845 by the ^{15}N RD data (Fig. S6c). For this reason, this data point was excluded for ^{1}H
846 CEST and $^{13}C/^{15}N$ RD comparison (Fig. 5a).
847
848 *Off-resonance ^{13}C $R_{1\rho}$ relaxation dispersion*: ^{13}C $R_{1\rho}$ experiments were performed
849 using 1D $R_{1\rho}$ schemes as described previously (Nikolova et al., 2012a; Nikolova
850 et al., 2011; Hansen et al., 2009). The spin-lock powers and offsets are listed in
851 Table S3. The spin-lock was applied for a maximal duration < 60 ms to achieve
852 ~70 % loss of peak intensity at the end of relaxation delay. Off-resonance $R_{1\rho}$
853 profiles (Fig. S8) were generated by plotting $(R_2 + R_{ex}) = (R_{1\rho} - R_1\cos^2\theta)/\sin^2\theta$,
854 where θ is the angle between the effective field of the observed resonance and the
855 z-axis, as a function of $\Omega_{eff}/2\pi$, where $\Omega_{eff} = \omega_{obs} - \omega_{RF}$, where ω_{obs} is the Larmor
856 frequency of the spin and ω_{RF} is the carrier frequency of the applied spin-lock.
857
858 *Fitting of ^{13}C $R_{1\rho}$ data:* 1D peak intensities were measured using NMRpipe
859 (Delaglio et al., 1995). $R_{1\rho}$ values for a given spin-lock power and offset were
860 calculated by fitting the intensities as a function of delay time to a mono-
861 exponential decay (Kimsey et al., 2015). A Monte-Carlo approach was used to
862 calculate the uncertainties of $R_{1\rho}$ (Bothe et al., 2014). Alignment of initial
863 magnetization during the Bloch-McConnell fitting was performed based on the

$k_{ex}/\Delta\omega$ value (Rangadurai et al., 2019b). Chemical exchange parameters were obtained by fitting experimental $R_{1\rho}$ values to numerical solutions of a 2-state Bloch-McConnell (B-M) equations (Mcconnell, 1958). A Monte-Carlo approach was used to calculate the errors of exchange parameters (Bothe et al., 2014) . Reduced chi-square ($r\chi^2$) was calculated to assess the goodness of fitting (Rangadurai et al., 2019b).

4.3 Thermodynamic Analysis

The observed temperature dependence of k_1, k_{-1} for the Watson-Crick to Hoogsteen exchange measuring using ^{1}H CEST were fit to a modified van't Hoff equation that accounts for statistical compensation effects and assumes a smooth energy surface as described previously (Nikolova et al., 2011; Coman and Russu, 2005):

$$\ln\left(\frac{k_i(T)}{T}\right) = \ln\left(\frac{k_B\kappa}{h}\right) - \frac{\Delta G_i^{\circ T}(T_{hm})}{RT_{hm}} - \frac{\Delta H_i^{\circ T}}{R}\left(\frac{1}{T} - \frac{1}{T_{hm}}\right) \quad (6)$$

k_i (i = 1, -1) is the forward and backward rate constants, $\Delta G_i^{\circ T}(T)$ and $\Delta H_i^{\circ T}$ are the free energy (at temperature T, in Kelvin) and enthalpy of activation (i = 1) or deactivation (i = -1) respectively. R is the universal gas constant (kcal mol^{-1} K^{-1})

and T_{hm} is the harmonic mean of the experimental temperatures (T_i in K) computed as $T_{hm} = n/\sum_{i=1}^{n}(1/T_i)$, k_B is the Boltzmann's constant (J K^{-1}), κ is the transmission coefficient (assumed to be unity) and h is the Planck constant (J s).

The goodness-of-fit indicator R^2 (coefficient of determination) (Fig. S6) between the measured and fitted rate constants was calculated as follows: $R^2 = 1 - \frac{SS_{res}}{SS_{total}}, SS_{res} = \sum(k_{i,fit} - k_{i,exp})^2$, $SS_{total} = \sum(k_{i,exp} - \overline{k_{i,exp}})^2$. $k_{i,fit}$ and $k_{i,exp}$ (i = 1, -1) are fitted and experimentally measured rate constants. $\overline{k_{i,exp}}$ is the mean of all $k_{i,exp}$. Errors of fitting for $\Delta G_i^{\circ T}$ and ΔH_i^T were calculated as the square root of the diagonal elements of the covariance matrix. $T\Delta S_i^T$ is calculated as $\Delta H_i^T - \Delta G_i^{\circ T}$.

Data and code availability. The data that support this study are contained in the published article (and its Supplementary Information) or are available from the corresponding author on reasonable request. The python scripts for ^{1}H CEST data fitting are available at https://github.com/alhashimilab/1H-CEST.

Author contributions. BL, AR, and HMA conceived the project and experimental design. BL, AR, and HS prepared the samples and set up the imino ^{1}H CEST experiment. BL performed ^{1}H CEST experiments and data analysis. HS performed ^{13}C $R_{1\rho}$ experiments. HMA, BL, and AR wrote the manuscript with critical input from HS.

Competing interests. The authors declare that they have no conflict of interest.

Acknowledgments. We thank Prof. Katja Petzold for sharing the ^{1}H CEST pulse sequence. We thank Dr. Or Szekely for general input and Ainan Geng for help with the ^{1}H inhomogeneity measurements.

Financial Support. This work was supported by the US National Institutes of Health (R01GM089846) Grants to H.M.A.

Reference

Afek, A., Shi, H., Rangadurai, A., Sahay, H., Senitzki, A., Xhani, S., Fang, M., Salinas, R., Mielko, Z., Pufall, M. A., Poon, G. M. K., Haran, T. E., Schumacher, M. A., Al-Hashimi, H. M., and Gordan, R.: DNA mismatches reveal conformational penalties in protein-DNA recognition, Nature, 587, 291-296, 10.1038/s41586-020-2843-2, 2020.

Aishima, J., Gitti, R. K., Noah, J. E., Gan, H. H., Schlick, T., and Wolberger, C.: A Hoogsteen base pair embedded in undistorted B-DNA, Nucleic acids research, 30, 5244-5252, 2002.

Alvey, H. S., Gottardo, F. L., Nikolova, E. N., and Al-Hashimi, H. M.: Widespread transient Hoogsteen base pairs in canonical duplex DNA with variable energetics, Nat Commun, 5, 4786, 10.1038/ncomms5786, 2014.

Baronti, L., Guzzetti, I., Ebrahimi, P., Friebe Sandoz, S., Steiner, E., Schlagnitweit, J., Fromm, B., Silva, L., Fontana, C., Chen, A. A., and Petzold, K.: Base-pair conformational switch modulates miR-34a targeting of Sirt1 mRNA, Nature, 583, 139-144, 10.1038/s41586-020-2336-3, 2020.

Ben Imeddourene, A., Zargarian, L., Buckle, M., Hartmann, B., and Mauffret, O.: Slow motions in A.T rich DNA sequence, Sci Rep, 10, 19005, 10.1038/s41598-020-75645-x, 2020.

Bothe, J. R., Stein, Z. W., and Al-Hashimi, H. M.: Evaluating the uncertainty in exchange parameters determined from off-resonance R1rho relaxation dispersion for systems in fast exchange, J Magn Reson, 244, 18-29, 10.1016/j.jmr.2014.04.010, 2014.

Bouvignies, G. and Kay, L. E.: Measurement of proton chemical shifts in invisible states of slowly exchanging protein systems by chemical exchange saturation transfer, J Phys Chem B, 116, 14311-14317, 10.1021/jp311109u, 2012.

Burnham, K. P. and Anderson, D. R.: Multimodel inference - understanding AIC and BIC in model selection, Sociol Method Res, 33, 261-304, 10.1177/0049124104268644, 2004.

Chen, B., LeBlanc, R., and Dayie, T. K.: SAM-II Riboswitch Samples at least Two Conformations in Solution in the Absence of Ligand: Implications for Recognition, Angew Chem Int Edit, 55, 2724-2727, 10.1002/anie.201509997, 2016.

Coman, D. and Russu, I. M.: A nuclear magnetic resonance investigation of the energetics of basepair opening pathways in DNA, Biophys J, 89, 3285-3292, 10.1529/biophysj.105.065763, 2005.

Czernek, J., Fiala, R., and Sklenar, V.: Hydrogen bonding effects on the (15)N and (1)H shielding tensors in nucleic acid base pairs, J Magn Reson, 145, 142-146, 10.1006/jmre.2000.2091, 2000.

Delaglio, F., Grzesiek, S., Vuister, G. W., Zhu, G., Pfeifer, J., and Bax, A.: NMRPipe: a multidimensional spectral processing system based on UNIX pipes, J Biomol NMR, 6, 277-293, 10.1007/BF00197809, 1995.

Dubini, R. C. A., Schon, A., Muller, M., Carell, T., and Rovo, P.: Impact of 5-formylcytosine on the melting kinetics of DNA by 1H NMR chemical exchange, Nucleic Acids Res, 48, 8796-8807, 10.1093/nar/gkaa589, 2020.

Eichmuller, C. and Skrynnikov, N. R.: A new amide proton R1rho experiment permits accurate characterization of microsecond time-scale conformational exchange, J Biomol NMR, 32, 281-293,

10.1007/s10858-005-0658-y, 2005.
Felsenfeld, G., Davies, D. R., and Rich, A.: Formation of a 3-Stranded Polynucleotide Molecule, Journal of the American Chemical Society, 79, 2023-2024, DOI 10.1021/ja01565a074, 1957.
Frank, A. T., Horowitz, S., Andricioaei, I., and Al-Hashimi, H. M.: Utility of 1H NMR chemical shifts in determining RNA structure and dynamics, J Phys Chem B, 117, 2045-2052, 10.1021/jp310863c, 2013.
Furukawa, A., Walinda, E., Arita, K., and Sugase, K.: Structural dynamics of double-stranded DNA with epigenome modification, Nucleic Acids Res, 49, 1152-1162, 10.1093/nar/gkaa1210, 2021.
Golovenko, D., Brauning, B., Vyas, P., Haran, T. E., Rozenberg, H., and Shakked, Z.: New Insights into the Role of DNA Shape on Its Recognition by p53 Proteins, Structure, 26, 1237-1250 e1236, 10.1016/j.str.2018.06.006, 2018.
Guenneugues, M., Berthault, P., and Desvaux, H.: A method for determining B1 field inhomogeneity. Are the biases assumed in heteronuclear relaxation experiments usually underestimated?, J Magn Reson, 136, 118-126, 10.1006/jmre.1998.1590, 1999.
Gueron, M. and Leroy, J. L.: Studies of base pair kinetics by NMR measurement of proton exchange, Methods Enzymol, 261, 383-413, 10.1016/s0076-6879(95)61018-9, 1995.
Gueron, M., Kochoyan, M., and Leroy, J. L.: A single mode of DNA base-pair opening drives imino proton exchange, Nature, 328, 89-92, 10.1038/328089a0, 1987.
Hansen, A. L., Lundstrom, P., Velyvis, A., and Kay, L. E.: Quantifying millisecond exchange dynamics in proteins by CPMG relaxation dispersion NMR using side-chain 1H probes, J Am Chem Soc, 134, 3178-3189, 10.1021/ja210711v, 2012.
Hansen, A. L., Nikolova, E. N., Casiano-Negroni, A., and Al-Hashimi, H. M.: Extending the range of microsecond-to-millisecond chemical exchange detected in labeled and unlabeled nucleic acids by selective carbon R(1rho) NMR spectroscopy, J Am Chem Soc, 131, 3818-3819, 10.1021/ja8091399, 2009.
Hoogsteen, K.: The Structure of Crystals Containing a Hydrogen-Bonded Complex of 1-Methylthymine and 9-Methyladenine, Acta Crystallogr, 12, 822-823, Doi 10.1107/S0365110x59002389, 1959.
Hwang, T. L. and Shaka, A. J.: Water Suppression That Works - Excitation Sculpting Using Arbitrary Wave-Forms and Pulsed-Field Gradients, J Magn Reson Ser A, 112, 275-279, DOI 10.1006/jmra.1995.1047, 1995.
Ishima, R. and Torchia, D. A.: Extending the range of amide proton relaxation dispersion experiments in proteins using a constant-time relaxation-compensated CPMG approach, J Biomol NMR, 25, 243-248, 10.1023/a:1022851228405, 2003.
Ishima, R., Wingfield, P. T., Stahl, S. J., Kaufman, J. D., and Torchia, D. A.: Using amide H-1 and N-15 transverse relaxation to detect millisecond time-scale motions in perdeuterated proteins: Application to HIV-1 protease, Journal of the American Chemical Society, 120, 10534-10542, DOI 10.1021/ja981546c, 1998.
Juen, M. A., Wunderlich, C. H., Nussbaumer, F., Tollinger, M., Kontaxis, G., Konrat, R., Hansen, D.

F., and Kreutz, C.: Excited States of Nucleic Acids Probed by Proton Relaxation Dispersion NMR Spectroscopy, Angew Chem Int Ed Engl, 55, 12008-12012, 10.1002/anie.201605870, 2016.
Kimsey, I. J., Petzold, K., Sathyamoorthy, B., Stein, Z. W., and Al-Hashimi, H. M.: Visualizing transient Watson-Crick-like mispairs in DNA and RNA duplexes, Nature, 519, 315-320, 10.1038/nature14227, 2015.
Kimsey, I. J., Szymanski, E. S., Zahurancik, W. J., Shakya, A., Xue, Y., Chu, C. C., Sathyamoorthy, B., Suo, Z., and Al-Hashimi, H. M.: Dynamic basis for dG*dT misincorporation via tautomerization and ionization, Nature, 554, 195-201, 10.1038/nature25487, 2018.
Kitayner, M., Rozenberg, H., Rohs, R., Suad, O., Rabinovich, D., Honig, B., and Shakked, Z.: Diversity in DNA recognition by p53 revealed by crystal structures with Hoogsteen base pairs, Nat Struct Mol Biol, 17, 423-429, 10.1038/nsmb.1800, 2010.
Lam, S. L. and Chi, L. M.: Use of chemical shifts for structural studies of nucleic acids, Prog Nucl Magn Reson Spectrosc, 56, 289-310, 10.1016/j.pnmrs.2010.01.002, 2010.
Lane, A. N., Bauer, C. J., and Frenkiel, T. A.: Determination of conformational transition rates in the trp promoter by 1H NMR rotating-frame T1 and cross-relaxation rate measurements, Eur Biophys J, 21, 425-431, 10.1007/BF00185870, 1993.
LeBlanc, R. M., Longhini, A. P., Tugarinov, V., and Dayie, T. K.: NMR probing of invisible excited states using selectively labeled RNAs, J Biomol NMR, 71, 165-172, 10.1007/s10858-018-0184-3, 2018.
Leijon, M. and Graslund, A.: Effects of sequence and length on imino proton exchange and base pair opening kinetics in DNA oligonucleotide duplexes, Nucleic Acids Res, 20, 5339-5343, 10.1093/nar/20.20.5339, 1992.
Leroy, J. L., Kochoyan, M., Huynh-Dinh, T., and Gueron, M.: Characterization of base-pair opening in deoxynucleotide duplexes using catalyzed exchange of the imino proton, J Mol Biol, 200, 223-238, 10.1016/0022-2836(88)90236-7, 1988.
Ling, H., Boudsocq, F., Plosky, B. S., Woodgate, R., and Yang, W.: Replication of a cis-syn thymine dimer at atomic resolution, Nature, 424, 1083-1087, 10.1038/nature01919, 2003.
Liu, B., Shi, H., Rangadurai, A., Nussbaumer, F., Chu, C. C., Erharter, K., Case, D. A., Kreutz, C., and Al-Hashimi, H. M.: A quantitative model predicts how m6A reshapes the kinetic landscape of nucleic acid hybridization and conformational transitions, bioRxiv, 2020.
Lu, L., Yi, C., Jian, X., Zheng, G., and He, C.: Structure determination of DNA methylation lesions N1-meA and N3-meC in duplex DNA using a cross-linked protein-DNA system, Nucleic Acids Res, 38, 4415-4425, 10.1093/nar/gkq129, 2010.
Lundstrom, P. and Akke, M.: Off-resonance rotating-frame amide proton spin relaxation experiments measuring microsecond chemical exchange in proteins, J Biomol NMR, 32, 163-173, 10.1007/s10858-005-5027-3, 2005.
Lundstrom, P., Hansen, D. F., Vallurupalli, P., and Kay, L. E.: Accurate measurement of alpha proton chemical shifts of excited protein states by relaxation dispersion NMR spectroscopy, Journal of the American Chemical Society, 131, 1915-1926, 10.1021/ja807796a, 2009.

Mcconnell, H. M.: Reaction Rates by Nuclear Magnetic Resonance, J Chem Phys, 28, 430-431, Doi 10.1063/1.1744152, 1958.
Nair, D. T., Johnson, R. E., Prakash, L., Prakash, S., and Aggarwal, A. K.: Hoogsteen base pair formation promotes synthesis opposite the 1,N6-ethenodeoxyadenosine lesion by human DNA polymerase iota, Nat Struct Mol Biol, 13, 619-625, 10.1038/nsmb1118, 2006.
Nikolova, E. N., Gottardo, F. L., and Al-Hashimi, H. M.: Probing transient Hoogsteen hydrogen bonds in canonical duplex DNA using NMR relaxation dispersion and single-atom substitution, J Am Chem Soc, 134, 3667-3670, 10.1021/ja2117816, 2012a.
Nikolova, E. N., Bascom, G. D., Andricioaei, I., and Al-Hashimi, H. M.: Probing Sequence-Specific DNA Flexibility in A-Tracts and Pyrimidine-Purine Steps by Nuclear Magnetic Resonance C-13 Relaxation and Molecular Dynamics Simulations, Biochemistry, 51, 8654-8664, 10.1021/bi3009517, 2012b.
Nikolova, E. N., Goh, G. B., Brooks, C. L., 3rd, and Al-Hashimi, H. M.: Characterizing the protonation state of cytosine in transient G.C Hoogsteen base pairs in duplex DNA, J Am Chem Soc, 135, 6766-6769, 10.1021/ja400994e, 2013a.
Nikolova, E. N., Kim, E., Wise, A. A., O'Brien, P. J., Andricioaei, I., and Al-Hashimi, H. M.: Transient Hoogsteen base pairs in canonical duplex DNA, Nature, 470, 498-502, 10.1038/nature09775, 2011.
Nikolova, E. N., Zhou, H., Gottardo, F. L., Alvey, H. S., Kimsey, I. J., and Al-Hashimi, H. M.: A historical account of Hoogsteen base-pairs in duplex DNA, Biopolymers, 99, 955-968, 10.1002/bip.22334, 2013b.
Otten, R., Villali, J., Kern, D., and Mulder, F. A.: Probing microsecond time scale dynamics in proteins by methyl (1)H Carr-Purcell-Meiboom-Gill relaxation dispersion NMR measurements. Application to activation of the signaling protein NtrC(r), J Am Chem Soc, 132, 17004-17014, 10.1021/ja107410x, 2010.
Palmer, A. G., 3rd: Chemical exchange in biomacromolecules: past, present, and future, J Magn Reson, 241, 3-17, 10.1016/j.jmr.2014.01.008, 2014.
Rangadurai, A., Shi, H., and Al-Hashimi, H. M.: Extending the Sensitivity of CEST NMR Spectroscopy to Micro-to-Millisecond Dynamics in Nucleic Acids Using High-Power Radio-Frequency Fields, Angew Chem Int Ed Engl, 59, 11262-11266, 10.1002/anie.202000493, 2020a.
Rangadurai, A., Kremser, J., Shi, H., Kreutz, C., and Al-Hashimi, H. M.: Direct evidence for (G)O6...H2-N4(C)(+) hydrogen bonding in transient G(syn)-C(+) and G(syn)-m(5)C(+) Hoogsteen base pairs in duplex DNA from cytosine amino nitrogen off-resonance R1rho relaxation dispersion measurements, J Magn Reson, 308, 106589, 10.1016/j.jmr.2019.106589, 2019a.
Rangadurai, A., Szymaski, E. S., Kimsey, I. J., Shi, H., and Al-Hashimi, H. M.: Characterizing micro-to-millisecond chemical exchange in nucleic acids using off-resonance R1rho relaxation dispersion, Prog Nucl Magn Reson Spectrosc, 112-113, 55-102, 10.1016/j.pnmrs.2019.05.002, 2019b.
Rangadurai, A., Shi, H., Xu, Y., Liu, B., Abou Assi, H., Zhou, H., Kimsey, I., and Al-Hashimi, H.: delta-Melt: Nucleic acid conformational penalties from melting experiments, bioRxiv, 2020b.
Rangadurai, A., Zhou, H., Merriman, D. K., Meiser, N., Liu, B., Shi, H., Szymanski, E. S., and Al-

Hashimi, H. M.: Why are Hoogsteen base pairs energetically disfavored in A-RNA compared to B-DNA?, Nucleic Acids Res, 46, 11099-11114, 10.1093/nar/gky885, 2018.
Sathyamoorthy, B., Lee, J., Kimsey, I., Ganser, L. R., and Al-Hashimi, H.: Development and application of aromatic [(13)C, (1)H] SOFAST-HMQC NMR experiment for nucleic acids, J Biomol NMR, 60, 77-83, 10.1007/s10858-014-9856-9, 2014.
Sathyamoorthy, B., Shi, H., Zhou, H., Xue, Y., Rangadurai, A., Merriman, D. K., and Al-Hashimi, H. M.: Insights into Watson-Crick/Hoogsteen breathing dynamics and damage repair from the solution structure and dynamic ensemble of DNA duplexes containing m1A, Nucleic Acids Res, 45, 5586-5601, 10.1093/nar/gkx186, 2017.
Schlagnitweit, J., Steiner, E., Karlsson, H., and Petzold, K.: Efficient Detection of Structure and Dynamics in Unlabeled RNAs: The SELOPE Approach, Chemistry, 24, 6067-6070, 10.1002/chem.201800992, 2018.
Schnieders, R., Wolter, A. C., Richter, C., Wohnert, J., Schwalbe, H., and Furtig, B.: Novel (13) C-detected NMR Experiments for the Precise Detection of RNA Structure, Angew Chem Int Ed Engl, 58, 9140-9144, 10.1002/anie.201904057, 2019.
Sekhar, A., Rosenzweig, R., Bouvignies, G., and Kay, L. E.: Hsp70 biases the folding pathways of client proteins, Proc Natl Acad Sci U S A, 113, E2794-2801, 10.1073/pnas.1601846113, 2016.
Shi, H., Clay, M. C., Rangadurai, A., Sathyamoorthy, B., Case, D. A., and Al-Hashimi, H. M.: Atomic structures of excited state A-T Hoogsteen base pairs in duplex DNA by combining NMR relaxation dispersion, mutagenesis, and chemical shift calculations, J Biomol NMR, 70, 229-244, 10.1007/s10858-018-0177-2, 2018.
Shi, H., Kimsey, I., Liu, H., Pham, U., Schumacher, M. A., and Al-Hashimi, H.: Revealing A-T and G-C Hoogsteen base pairs in stressed protein-bound duplex DNA, bioRxiv, 2021.
Shi, H., Liu, B., Nussbaumer, F., Rangadurai, A., Kreutz, C., and Al-Hashimi, H. M.: NMR Chemical Exchange Measurements Reveal That N(6)-Methyladenosine Slows RNA Annealing, J Am Chem Soc, 141, 19988-19993, 10.1021/jacs.9b10939, 2019.
Singh, U. S., Moe, J. G., Reddy, G. R., Weisenseel, J. P., Marnett, L. J., and Stone, M. P.: 1H NMR of an oligodeoxynucleotide containing a propanodeoxyguanosine adduct positioned in a (CG)3 frameshift hotspot of Salmonella typhimurium hisD3052: Hoogsteen base-pairing at pH 5.8, Chem Res Toxicol, 6, 825-836, 10.1021/tx00036a012, 1993.
Smith, C. A., Ban, D., Pratihar, S., Giller, K., Schwiegk, C., de Groot, B. L., Becker, S., Griesinger, C., and Lee, D.: Population shuffling of protein conformations, Angew Chem Int Ed Engl, 54, 207-210, 10.1002/anie.201408890, 2015.
Snoussi, K. and Leroy, J. L.: Imino proton exchange and base-pair kinetics in RNA duplexes, Biochemistry, 40, 8898-8904, 10.1021/bi010385d, 2001.
Sripakdeevong, P., Cevec, M., Chang, A. T., Erat, M. C., Ziegeler, M., Zhao, Q., Fox, G. E., Gao, X., Kennedy, S. D., Kierzek, R., Nikonowicz, E. P., Schwalbe, H., Sigel, R. K., Turner, D. H., and Das, R.: Structure determination of noncanonical RNA motifs guided by (1)H NMR chemical shifts, Nature methods, 11, 413-416, 10.1038/nmeth.2876, 2014.

Steiner, E., Schlagnitweit, J., Lundstrom, P., and Petzold, K.: Capturing Excited States in the Fast-Intermediate Exchange Limit in Biological Systems Using (HNMR)-H-1 Spectroscopy, Angew Chem Int Edit, 55, 15869-15872, 10.1002/anie.201609102, 2016.

Stelling, A. L., Xu, Y., Zhou, H., Choi, S. H., Clay, M. C., Merriman, D. K., and Al-Hashimi, H. M.: Robust IR-based detection of stable and fractionally populated G-C(+) and A-T Hoogsteen base pairs in duplex DNA, FEBS Lett, 591, 1770-1784, 10.1002/1873-3468.12681, 2017.

Swails, J., Zhu, T., He, X., and Case, D. A.: AFNMR: automated fragmentation quantum mechanical calculation of NMR chemical shifts for biomolecules, Journal of biomolecular NMR, 63, 125-139, 10.1007/s10858-015-9970-3, 2015.

Tateishi-Karimata, H., Nakano, M., and Sugimoto, N.: Comparable stability of Hoogsteen and Watson-Crick base pairs in ionic liquid choline dihydrogen phosphate, Sci Rep, 4, 3593, 10.1038/srep03593, 2014.

Ughetto, G., Wang, A. H., Quigley, G. J., van der Marel, G. A., van Boom, J. H., and Rich, A.: A comparison of the structure of echinomycin and triostin A complexed to a DNA fragment, Nucleic Acids Res, 13, 2305-2323, 10.1093/nar/13.7.2305, 1985.

Wang, A. H., Ughetto, G., Quigley, G. J., Hakoshima, T., van der Marel, G. A., van Boom, J. H., and Rich, A.: The molecular structure of a DNA-triostin A complex, Science, 225, 1115-1121, 10.1126/science.6474168, 1984.

Wang, S., Song, Y., Wang, Y., Li, X., Fu, B., Liu, Y., Wang, J., Wei, L., Tian, T., and Zhou, X.: The m(6)A methylation perturbs the Hoogsteen pairing-guided incorporation of an oxidized nucleotide, Chem Sci, 8, 6380-6388, 10.1039/c7sc02340e, 2017.

Wang, Y., Han, G., Jiang, X., Yuwen, T., and Xue, Y.: Chemical shift prediction of RNA imino groups: application toward characterizing RNA excited states, Nat Commun, 12, 1595, 10.1038/s41467-021-21840-x, 2021.

Wang, Y. S. and Ikuta, S.: Proton on-Resonance Rotating Frame Spin-Lattice Relaxation Measurements of B and Z Double-Helical Oligodeoxyribonucleotides in Solution, Journal of the American Chemical Society, 111, 1243-1248, DOI 10.1021/ja00186a013, 1989.

Weininger, U., Liu, Z., McIntyre, D. D., Vogel, H. J., and Akke, M.: Specific 12CbetaD(2)12CgammaD(2)S13CepsilonHD(2) isotopomer labeling of methionine to characterize protein dynamics by 1H and 13C NMR relaxation dispersion, J Am Chem Soc, 134, 18562-18565, 10.1021/ja309294u, 2012.

Weininger, U., Blissing, A. T., Hennig, J., Ahlner, A., Liu, Z., Vogel, H. J., Akke, M., and Lundstrom, P.: Protein conformational exchange measured by 1H R1rho relaxation dispersion of methyl groups, J Biomol NMR, 57, 47-55, 10.1007/s10858-013-9764-4, 2013.

Xu, Y., McSally, J., Andricioaei, I., and Al-Hashimi, H. M.: Modulation of Hoogsteen dynamics on DNA recognition, Nat Commun, 9, 1473, 10.1038/s41467-018-03516-1, 2018.

Xu, Y., Manghrani, A., Liu, B., Shi, H., Pham, U., Liu, A., and Al-Hashimi, H. M.: Hoogsteen base pairs increase the susceptibility of double-stranded DNA to cytotoxic damage, J Biol Chem, 295, 15933-15947, 10.1074/jbc.RA120.014530, 2020.

Yamazaki, T., Muhandiram, R., and Kay, L. E.: NMR Experiments for the Measurement of Carbon Relaxation Properties in Highly Enriched, Uniformly 13C,15N-Labeled Proteins: Application to 13C.alpha. Carbons, Journal of the American Chemical Society, 116, 8266-8278, 10.1021/ja00097a037, 1994.

Yuwen, T., Sekhar, A., and Kay, L. E.: Separating Dipolar and Chemical Exchange Magnetization Transfer Processes in (1) H-CEST, Angew Chem Int Ed Engl, 56, 6122-6125, 10.1002/anie.201610759, 2017a.

Yuwen, T. R., Huang, R., and Kay, L. E.: Probing slow timescale dynamics in proteins using methyl H-1 CEST, Journal of Biomolecular Nmr, 68, 215-224, 10.1007/s10858-017-0121-x, 2017b.

Zhao, B., Hansen, A. L., and Zhang, Q.: Characterizing slow chemical exchange in nucleic acids by carbon CEST and low spin-lock field R(1rho) NMR spectroscopy, J Am Chem Soc, 136, 20-23, 10.1021/ja409835y, 2014.

Zhou, H., Sathyamoorthy, B., Stelling, A., Xu, Y., Xue, Y., Pigli, Y. Z., Case, D. A., Rice, P. A., and Al-Hashimi, H. M.: Characterizing Watson-Crick versus Hoogsteen Base Pairing in a DNA-Protein Complex Using Nuclear Magnetic Resonance and Site-Specifically (13)C- and (15)N-Labeled DNA, Biochemistry, 58, 1963-1974, 10.1021/acs.biochem.9b00027, 2019.

Zhou, H., Kimsey, I. J., Nikolova, E. N., Sathyamoorthy, B., Grazioli, G., McSally, J., Bai, T., Wunderlich, C. H., Kreutz, C., Andricioaei, I., and Al-Hashimi, H. M.: m(1)A and m(1)G disrupt A-RNA structure through the intrinsic instability of Hoogsteen base pairs, Nature structural & molecular biology, 23, 803-810, 10.1038/nsmb.3270, 2016.

Zimmer, D. P. and Crothers, D. M.: NMR of enzymatically synthesized uniformly 13C15N-labeled DNA oligonucleotides, Proc Natl Acad Sci U S A, 92, 3091-3095, 10.1073/pnas.92.8.3091, 1995.